

AMERICAN UNIVERSITY OF BEIRUT

THERMAL CREEP BEHAVIOR OF STEEL FRAMES WITH
SHEAR TAB CONNECTIONS UNDER TRANSIENT-STATE
CONDITIONS OF FIRE

by
KARIM KHALED AL KHATIB

A thesis
submitted in partial fulfillment of the requirements
for the degree of Master of Engineering
to the Department of Civil and Environmental Engineering
of the Maroun Semaan Faculty of Engineering and Architecture
at the American University of Beirut

Beirut, Lebanon
August 2018

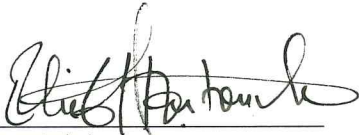
AMERICAN UNIVERSITY OF BEIRUT

THERMAL CREEP BEHAVIOR OF STEEL FRAMES WITH
SHEAR TAB CONNECTIONS UNDER TRANSIENT-STATE
CONDITIONS OF FIRE

by
KARIM KHALED AL KHATIB


Approved by:

Dr. Elie G. Hantouche, Assistant Professor
Department of Civil and Environmental Engineering



Advisor

Dr. Ghassan R. Chehab, Associate Professor
Department of Civil and Environmental Engineering



Member of Committee

Dr. George A. Saad, Associate Professor
Department of Civil and Environmental Engineering



Member of Committee

Date of thesis defense: August 1, 2018

AMERICAN UNIVERSITY OF BEIRUT

THESIS, DISSERTATION, PROJECT RELEASE FORM

Student Name: Al Khatib Karim Khaled
Last First Middle

Master's Thesis Master's Project Doctoral Dissertation

I authorize the American University of Beirut to: (a) reproduce hard or electronic copies of my thesis, dissertation, or project; (b) include such copies in the archives and digital repositories of the University; and (c) make freely available such copies to third parties for research or educational purposes.

I authorize the American University of Beirut, to: (a) reproduce hard or electronic copies of it; (b) include such copies in the archives and digital repositories of the University; and (c) make freely available such copies to third parties for research or educational purposes after:

One ---- year from the date of submission of my thesis, dissertation, or project.

Two ---- years from the date of submission of my thesis, dissertation, or project.

Three ~~---/~~ years from the date of submission of my thesis, dissertation, or project.



Signature

August 28, 2018

Date

ACKNOWLEDGMENTS

I would first like to thank my thesis advisor Dr. Elie Hantouche. The door to Dr. Hantouche's office was always open whenever I ran into a trouble spot or had a question about my research or writing. I appreciate his constant support and valuable critics which helped me develop my research skills, and knowledge throughout the time I spent at the American University of Beirut.

I would like to thank Dr. Mohammed Ali Morovat, Research Scientist Associate at the University of Texas at Austin, for his valuable efforts, time, and helpful discussions throughout the research.

My recognition and gratitude are also extended to my thesis committee, Dr. Ghassan Chehab and Dr. George Saad, for their encouragement and insightful comments. The graduate courses I attended with them were very beneficial in developing my research work.

I would like to acknowledge the financial support provided by the American University of Beirut Research Board under the grant No. 23310-103371.

I must express my very profound gratitude to my parents, brother, and sisters and also to my fiancé, Nessrine, and her lovely family. I would also like to thank my friends and research team; it was great sharing the workspace with all of you during the last two years. This accomplishment would not have been possible without your unfailing support. Thank you.

AN ABSTRACT OF THE THESIS OF

Karim Khaled Al Khatib for Master of Engineering
Major: Civil and Environmental Engineering

Title: Thermal Creep Behavior of Steel Frames with Shear Tab Connections under Transient-State Conditions of Fire

This study aims to investigate the behavior of full-scale steel frames with shear tab connections subjected to fire. It is often stated that creep (time-dependent) material of the steel can significantly influence the overall response of steel structures when subjected to fire temperatures. To address this issue, the effect of thermal creep of steel on the behavior of steel frames with shear tab connections due to fire temperatures is investigated. First, the study presents a methodology for explicit modeling of creep of structural steel in the ABAQUS finite element (FE) models under transient temperature conditions representative of building fires. Starting from existing creep model, the equations describing the time-dependent strains are derived and used to develop a new user-defined subroutine as per ABAQUS documentations. The development of this subroutine is presented through different stages which reflect the transition from conducting a steady-state analysis to a transient-state analysis.

FE models of full-scale steel frames with shear tab connections are first developed in ABAQUS. Then, the models are validated by comparing predictions from the FE analyses with experimental work available in literature. Afterwards, the time-dependent behavior of the validated FE models is investigated by explicitly including the thermal creep strains via the developed subroutine. Moreover, parametric studies are carried out to study the effect of key geometrical parameters and heating conditions on the overall response of steel frames in fire. These parameters are heating rate, column size, cooling duration, initial cooling temperature, beam geometry, and shear tab location.

The outcome of this study clearly emphasizes the importance of accounting for the creep effect in the structural-fire analyses of steel structures and shows that ignoring its effect can impose a major threat on the safety and integrity of steel structures when subjected to fire.

CONTENTS

ACKNOWLEDGMENTS	V
ABSTRACT	VI
ILLUSTRATIONS	IX
TABLES	XI
ABBREVIATIONS	XII
Chapter	
I. INTRODUCTION.....	1
II. THERMAL CREEP OF STRUCTURAL STEEL.....	8
A. Thermal Creep Phenomenon	8
B. Creep models in literature.....	9
C. Development of creep strains	10
III. DEVELOPMENT OF THE METHODOLOGY	13
A. Formulation of thermal creep of steel.....	13
B. Temperature environments	19
1. Steady-state temperature environment	19
2. Stepwise steady-state temperature environment	19
3. Transient-state temperature environment.....	20
C. Testing the subroutine	23
IV. FE MODELING OF SHEAR TAB CONNECTION ASSEMBLY	25
A. Development of the FE models	26
1. Geometry of the structural components	26
2. Material properties	27
3. Model discretization.....	28
4. Applied loads and boundary conditions.....	28

5. Temperature profile.....	29
B. Discussion of the results	30
V. EFFECT OF THERMAL CREEP ON THE SHEAR TAB ASSEMBLY RESPONSE.....	34
A. Time-dependent simulations: steady-state temperature environment	35
B. Time-dependent simulations: stepwise steady-state temperature environment	39
C. Time-dependent simulations: transient-state temperature environment.....	41
1. Parametric studies	42
a. Heating rate	42
b. Column size.....	44
c. Cooling duration.....	45
d. Initial cooling temperature	47
e. Beam geometry.....	48
f. Shear tab location	49
VI. SUMMARY, CONCLUSIONS AND RECOMMENDATIONS	51
A. Summary and Conclusions	51
B. Recommendations	53
BIBLIOGRAPHY	55
Appendix	
ABAQUS USER-DEFINED SUBROUTINES (CREEP).....	59
A. Steady-state analysis (for 550 °C)	59
B. Stepwise steady-state analysis	60
C. Transient-state analysis.....	61
LIST OF THE FE SIMULATIONS.....	62

ILLUSTRATIONS

Figure		Page
1.	Typical creep curve of structural steel	9
2.	Fields and Fields creep model of structural steel (1989)	14
3.	Creep response when changing stress or/and temperature (a) using time hardening formulation; (b) using strain hardening formulation	16
4.	Flowchart representing the subroutine incremental solution	22
5.	FE vs. mechanical model results: (a) trial model used to test the subroutine; (b) unloading scenario; (c) reverse loading scenario	24
6.	<i>Maxwell</i> model	24
7.	Details on the fire tests steel frames assembly of Wang et al. (2011)	26
8.	Details of the shear tab connection	27
9.	Detail of the full-scale steel frame FE model assembly	30
10.	Comparison between the experimental and FE model results: (a) beam axial force; (b) beam mid-span deflection	32
11.	Shear tab connection behavior: (a) before bolt contact; (b) after bolt contact; (c) bolt hole ovalization (elongation); (d) modeling of shear bolts	32
12.	Comparison between FE simulation and experimental (Wang et al., 2011) deformed shapes after the fire test: (a) Test 1; (b) Test 6	33
13.	Beam axial force of steady-state analysis at different temperatures versus (a) temperature; (b) time	36
14.	Beam mid-span deflection of steady-state analysis at different temperatures versus (a) temperature; (b) time	36
15.	Axial stress distribution over the cross-section when subjected to constant bending moment, before and after creep	38
16.	Axial stress distribution over the cross-section of the beam at the mid-span (creep starts at 500 °C): (a) at different depths versus time; (b) at the end of loading; (c) at the end of heating; (d) at the end of creep	39

17.	Stepwise steady-state temperature with and without including creep effect: (a) beam axial force; (b) mid-span deflection	40
18.	3D Representation of creep strain-time-temperature curves corresponding to the constant stress of 100 MPa (Fields & Fields 1989)	41
19.	Results obtained from ABAQUS of different heating rates for Tests 1 and 6: (a) beam axial force; (b) beam mid-span deflection	44
20.	Connection rotation results for different heating rates	45
21.	Beam axial force and mid-span deflection response for different cooling durations after: (a) fast heating (without creep); (b) heating rate of 20 °C/min	47
22.	Results for varying initial cooling temperatures following a heating rate of 20 °C/min: (a) beam axial force; (b) beam mid-span deflection	48
23.	Results of UB 305 × 102 × 25 beam for different heating rates: (a) beam axial force; (b) beam mid-span deflection	49
24.	Results of UB 305 × 102 × 25 beam with different shear tab locations: (a) beam axial force; (b) beam mid-span deflection	50

TABLES

Table		Page
1.	Summary of the frame assembly components properties	25
2.	Summary of the FE simulations developed in ABAQUS	62

ABBREVIATIONS

a , b , and c	temperature-dependent constants used in Fields and Fields (1989)
A , m , and n	temperature-dependent coefficients
E	elastic modulus of steel material
f_y and f_u	yielding and ultimate strength of steel
G	shear modulus
L	specimen length
T	temperature
t	time
α	coefficient of thermal expansion
σ	mechanical stress
ε_T	total strain
ε_e	elastic time-independent strains
ε_p	plastic time-independent strains
ε_{th}	thermal time-independent strains
ε_c	thermal creep time-dependent strain
τ	shear stress
γ	shear strain defined as: $\gamma_{ij} = 2\varepsilon_{ij}$
σ_v and ε_v	von Mises (equivalent) stress and strain
ν	<i>Poisson's</i> ratio

Special Symbols

\dot{x}	denotes a derivative of x with respect to time (rate)
Δ	prefixed to other term denotes an increment or change
$\frac{\partial}{\partial x}$	denotes partial differentiation with respect to x
$\int_a^b dx$	denotes definite integral from a to b with respect to x
$[]$	denotes a matrix

CHAPTER I

INTRODUCTION

Structural fire safety is one of the important aspects that should be considered when designing high-rise steel structures. During their life-time, steel structures are vulnerable to fire disasters that can impose a critical threat on the structure and life safety. Steel material is well known for having a good performance by means of high strength, stiffness and ductility at ambient temperatures. However, in fire, steel material experiences severe strength and stiffness degradation in addition to the induced thermal loads.

Steel connections play an important role in providing structural stability and integrity. Failure of one or more of these connections can lead to partial or total structural collapse. Until recently, steel connections were considered to have a higher fire resistance than that of the connected members; owing to the assumption that connection region has a smaller section factor (surface area divided by the volume per unit length) which makes it less vulnerable to fire temperatures. This assumption was proven to be misleading based on experiments (Newman et al. 2000; Wald et al. 2006; Wang et al. 2011) and through investigation of many fire disasters (Sunder et al. 2005), which reported that progressive structural collapse is mainly initiated by connection failure. This can be attribute to the fact that, in fire events, connection regions are subjected to additional stresses that are often not considered in conventional structural design. These additional stresses are mainly due to restrained thermal expansion and contraction, thermal gradient, and beam catenary action. Simple (shear) steel beam-column connections are extensively used in steel structures due to the ease of construction and fabrication. They are usually

considered, by designers, as ideally pinned joints that allow relative rotation and completely prevent the transition of bending moment between the connected structural members. However, in fire events, these connections exhibit a complex response, and studying their behavior under fire conditions is of great importance. A commonly used simple steel beam-column connection in the US is the shear tab connection. The shear tab connection, also called single/fin plate connection, is a steel plate welded to the column and bolted to the beam web. It is known that this type of connection has a high rotational capacity and provides high ductility mainly due to elongation of holes in bearing (Wald et al. 2006). Ductility of steel connections is a very important factor for the survival of steel beams in fire events by contributing to the redistribution of forces between supporting regions. Redistribution of forces can delay or prevent the beam failure and results in a ductile performance which is more favorable in fire events than a brittle failure (Pakala & Kodur 2016).

Extensive experimental and numerical studies were carried out to study the performance of isolated steel connections at elevated temperatures (Hu & Engelhardt 2014; Sleiman & Hantouche 2015; Yu et al. 2009a; Yu et al. 2009b). In fire, however, the behavior of steel connections is highly controlled by the interaction with the connected members (beams and columns) and also with the neighboring unheated members. Therefore, designing steel connections to withstand different fire scenarios should consider the interactions between members in structural frame systems rather than treating the connections as isolated structural elements.

To model the effect of temperature on mechanical properties of structural steel, conventional fire design methods use the concept of retention factors ($E_T / E_{20^\circ C}$, $f_{y,T} / f_{y,20^\circ C}$, and $f_{u,T} / f_{u,20^\circ C}$) that are solely dependent on the instant temperature of

steel (EN 1995-1-2 2005; Lie 1992; Poh 2001). However, the stress-strain behavior of structural steel at elevated temperatures is shown to be time-dependent for stresses and temperatures representative of building fires (Morovat 2014; Torić et al. 2013b). That is, at elevated temperature, the steel behavior is greatly influenced by the development of time-dependent strains, well known as thermal creep strains. Thermal creep (viscoplastic) strains are time-dependent inelastic strains which cause permanent structural deformations. When steel temperature exceeds around one-third of its melting point accompanied with applied stresses, the creep effect becomes significant and can greatly influence the overall structural behavior (Torić et al. 2013b). The creep phenomenon can be clearly observed through the increase in the mechanical strain when applying a sustained mechanical stress for a specific period of time under fire temperatures. On the contrary, relaxation phenomenon is observed through the stress reduction when applying a constant deformation for a specific time exposure to high temperatures.

It was not until recently that the time-dependent behavior of steel structures in fire received more attention from researchers (El Ghor et al. 2016; Morovat et al. 2014; Torić et al. 2013a) who reported that time is an important factor that should be considered in the analyses of steel structures in fire. Although some of the stress-strain-temperature curves readily available in design codes (e.g. EN 1995-1-2 2005) consider creep strains implicitly, recent studies showed that explicit consideration is more appropriate and can result in more accurate representation of the real case (Kodur & Dwaikat 2010; Kodur et al. 2010). The assessment of the fire resistance of steel connections should be carried out based on its performance in full-scale systems, or in other words, performance-based design approach. Accurate predictions of performance-based design approach depend on realistic and reliable representation of both loading conditions and material behavior. For

that reason, it is essential to include thermal creep effect, which is significant at high temperatures, when analyzing the structural fire resistance.

A review of literature shows that accurate predictions of structural response require the inclusion of thermal creep effect in the analyses (Kodur et al. 2010). Several experimental and numerical studies were conducted to further understand the time-dependent response of steel structures when subjected to fire temperatures. The influence of thermal creep of structural steel on the fire response of steel members and assemblies has been recognized in previous studies that observed a better agreements between experimental and computational predictions when the thermal creep was explicitly modeled in the FE simulations (Dwaikat & Kodur 2010; Huang et al. 2006; Kodur & Dwaikat 2010; Li & Zhang 2012; Morovat et al. 2011; Morovat et al. 2018; Yang & Yu 2013). It was shown in these studies that the behavior of structural steel elements can be highly time-dependent depending on the load conditions, duration of exposure to fire, and temperature magnitudes. For instance, in a series of fire buckling tests on ASTM A992 steel columns, Morovat et al. (2011; 2014) showed how the buckling strength of steel columns became time-dependent as a result of thermal creep of steel. It was shown that the column buckling does not depend only on the slenderness and the steel temperature, but also on the duration at which the load is applied. Similar time-dependent buckling phenomenon was observed by Yang and Yu (2013) during experiments on centrally loaded steel columns made of SN490FR fire-resistant steel. It was found that temperature, applied load, and slenderness ratio have a great impact on the buckling time. Torić et al. (2013b) showed an example of unrestrained steel beam subjected to fire temperatures up to (600 °C) for about 110 min. The results showed that including creep effect improves the predictions of the beam response compared to experimental results. Also, studies by

Kodur and Dwaikat (2010), using ANSYS creep models, proved that the explicit consideration of thermal creep resulted in more accurate predictions of restraint beams response under fire. Furthermore, Kodur et al. (2010) made a comparison between different material models available in literature including the Eurocode 3 (2005) temperature-stress-strain relationships. The results show that when effect of creep is explicitly considered, the predicted deflections compared well with the experimental results. Moreover, when using the Eurocode temperature-stress-strain relationships, which considers the creep effect implicitly, the analysis showed a conservative predictions of beam deflections when compared with the experimental results. Further, previous studies carried out FE simulations to investigate the effect of creep on isolated connections at elevated temperatures, and proposed a methodology to quantify the time-dependent behavior of these connections in the form of isochronous curves (El Ghor et al. 2016; Jabotian & Hantouche 2018; Morovat et al. 2018). The results showed that, in addition to the increase in the connection rotation, including creep effect can alter the failure mode. The National Institute of Standard and Technology (NIST) in its study of WTC building collapse in September 11, 2001 recognized the importance of thermal creep of steel (Luecke et al. 2005; Sunder et al. 2005). Therefore, creep was considered in all the simulations of the WTC building collapse to model both columns and floor trusses.

As indicated in previous studies, implementing creep material models in computational tools allows the explicit evaluation of the time- and temperature-dependent response of steel members and assemblies at elevated temperatures. This quantification of structural behavior in terms of both temperature and time is of utmost importance in developing performance-based design frameworks for the fire safety of steel structures.

Therefore, the primary goal of this study is to show how material creep models developed using creep tests can be utilized in analysis of steel structures exposed to the transient-state temperature conditions of fire. This study describes a methodology to consider the creep effects on the behavior of steel structures exposed to changing temperatures of fire. To consider the thermal creep of structural steel under transient-state temperature conditions, a user-defined subroutine is developed and implemented in computational analyses using the general-purpose FE software ABAQUS. The development of the subroutine is based on Fields and Fields (1989) constitutive creep model of ASTM A36 steel and follows available ABAQUS documentations (*ABAQUS ver. 6.14 documentation* 2014). To better understand and show the capability of the proposed methodology in predicting time-dependent behavior of steel structures under varied temperatures, three distinctive temperature environments were considered: steady-state, stepwise steady-state, and transient-state temperature environments. First, FE models of full-scale frames with shear tab connections are conducted using ABAQUS under transient-state analyses and validated against the experimental work done by Wang et al. (2011). Upon acquiring the validated conditions, FE models of the connection assembly are further generated and used to conduct an extensive parametric study of key parameters that affect the time-dependent behavior of the system during the heating and cooling phases of fire. These parameters are heating rate, column size, cooling duration, initial cooling temperature, beam geometry, and shear tab location.

The results obtained from the FE models give more insights on the effect of thermal creep on the steel frames with shear tab connections. This study also sheds light on the importance of explicit consideration of time in predicting the response of connection assemblies at different stages in the evolution of a structural-fire. To this aim,

the results obtained from the FE models are compared, discussed and analyzed to understand the impact mechanism of thermal creep on steel structures, specifically steel frames with shear tab connections.

CHAPTER II

THERMAL CREEP OF STRUCTURAL STEEL

A. Thermal Creep Phenomenon

The thermal creep behavior of steel is defined as the time-dependent inelastic strain of structural steel resulting from the application of both stress and temperature. In fact, at high temperatures, creep strains can even develop under stresses that are less than the yielding stress of steel. Creep strains occur due to the tendency of slip plane, at the grain level of steel, to move or dislocate under the influence of applied stress. Steel material contains defects within its crystalline structure that causes microstructural rearrangements including dislocation movement at high temperatures. Vacancies in the crystal structure can diffuse in the direction of stress causing progressive plastic deformations to occur (Kodur & Dwaikat 2010; Naumenko & Altenbach 2007). It was observed in many studies that deformations become time-dependent when temperature of steel reaches roughly one-third of its melting point (Torić et al. 2013b).

Studying the thermal creep phenomenon of structural steel is commonly established by conducting steady-state creep material tests in tension. In these tests, this phenomenon is observed through the increase in mechanical strain under the conditions of sustained mechanical stresses and constant temperatures. In most cases, creep curves can be divided into three stages with respect to time, as shown in Fig. 1. Once the load is applied, a primary stage takes place which is described by high creep rate that decreases with time due to work hardening. The secondary stage is associated with slow but steady rate through time. This is due to the balance between work hardening and thermal softening. Finally, prior to failure, deformation rate increases exponentially, because of

necking phenomena, until the specimen ruptures; this stage is denoted by tertiary stage. The tertiary stage is usually not recognized in creep models since it implies impending failure (Kodur & Dwaikat 2010; Li & Zhang 2012). Therefore, only the primary and secondary stages of creep are included in the structural fire analyses.

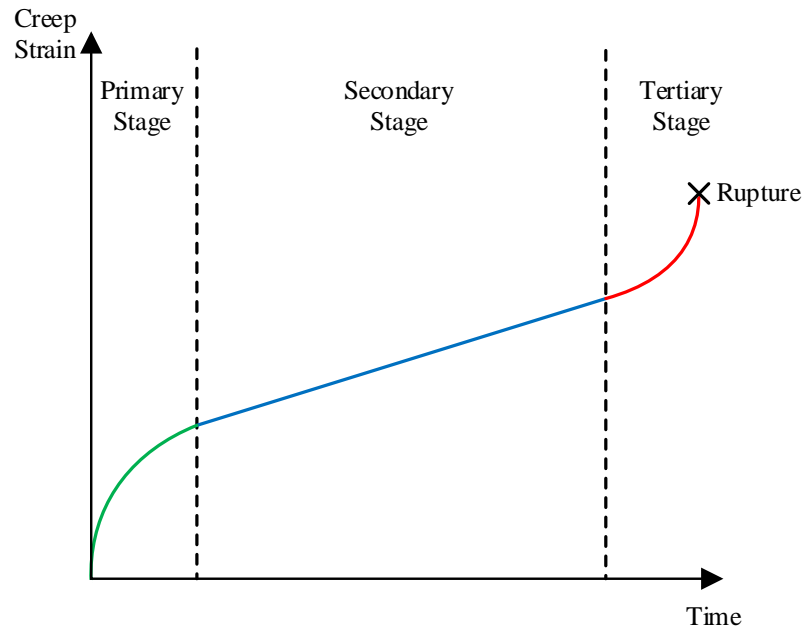


Figure. 1. Typical creep curve of structural steel.

B. Creep models in literature

Explicit inclusion of the creep effect in FE packages, such as ABAQUS and ANSYS, requires well-defined constitutive creep models capable of predicting the development of time-dependent strains under different conditions of temperatures and stresses. These models can be established based on material creep tests (Fields & Fields 1989; Matar et al. 2014; Wang et al. 2016). The resulting equations describe the creep behavior by an equivalent uniaxial behavior. Harmathy (1967) developed a model that predicts the time-dependent strains for ASTM A36 steel under elevated temperatures (up

to 700 °C). Many existing work used Harmathy (1967) model to introduce the creep effect into FE simulations (Huang & Tan 2004; Tan et al. 2002; Torić et al. 2013a). However, this model is limited to cases where stress is assumed constant. To address this shortcoming, many empirical models (Fields & Fields 1989; Kodur & Dwaikat 2010; Williams-leir 1983) are developed based on experimental tests. These models are developed through fitting experimental data into equations that can take different forms (e.g. power law, exponential law...) depending on the material behavior. For example, Fields and Fields (1989) used tensile and creep tests available in literature to study the deformation mechanism of ASTM A36 steel. The total strain was divided into different components where creep strain was considered as an explicit/independent component.

C. Development of creep strains

The total strain is the summation of both thermal and mechanical strains that can be divided into time-dependent and time-independent strains. In general, when considering creep strain as an independent component, the total strain can be written as follows:

$$\varepsilon_T = \varepsilon_e(\sigma, T) + \varepsilon_p(\sigma, T) + \varepsilon_{th}(T) + \varepsilon_c(t, \sigma, T) \quad (1)$$

where ε_T is the total strain, ε_e is the elastic time-independent strain, ε_p is the plastic time-independent strain, ε_{th} is the free thermal strain, and ε_c is the creep (plastic time-dependent) strain. The two components ε_e and ε_p are dependent on the instant temperature (T) and stress (σ), ε_{th} is dependent on the temperature, and ε_c is time (t), stress, and temperature dependent. Thus, the total deformation, ΔL , of a specimen of length L subjected to uniaxial stress can be expressed as:

$$\Delta L(t) = \int_0^L (\varepsilon_e + \varepsilon_p + \varepsilon_{th}) dx + \int_0^L \int_0^t \dot{\varepsilon}_c dt dx \quad (2)$$

where $\dot{\varepsilon}_c$ is the creep strain rate (strain per time).

In fire events, steel structures are subjected to strongly variable conditions which make analytical solution very complex, thus resorting to numerical solutions. In numerical analysis, such as the FE analysis, the change in the total strain ($\Delta\varepsilon_T$) within a given time step (Δt), in the explicit form, can be represented as:

$$\Delta\varepsilon_T = \frac{\sigma_{i+1}E_i - \sigma_i E_{i+1}}{E_i E_{i+1}} + \Delta\varepsilon_p + \Delta T \alpha + \dot{\varepsilon}_c \Delta t \quad (3)$$

where E is the temperature-dependent modulus of elasticity and α is the temperature dependent coefficient of thermal expansion. $\Delta\varepsilon_p$, and ΔT are the change in plastic (time-independent) strain and the change in temperature within the time step, respectively. In stationary (steady-state) creep tests, the stress and temperature are held constant, thus the change in the total strain, assuming no change in the cross-section area, is purely creep strain and Eq. (3) reduces to:

$$\Delta\varepsilon_T = \dot{\varepsilon}_c \Delta t \quad (4)$$

On the other hand, relaxation tests require applying a constant strain (deformation) and recording the change in the stress under constant temperature. That is, no change in the total strain ($\Delta\varepsilon_T = 0$) is permitted in relaxation tests. Thus, the change in stress, $\Delta\sigma$, within a given time step can be represented as:

$$\Delta\sigma = -\dot{\varepsilon}_c \Delta t E \quad (5)$$

As can be seen from Eq. (5), the creep strains result in a decrease in the stress, also called stress relaxation, as time increases. Although describing the material testing

behavior, these equations can give more insights on the impact mechanism of creep strains on the global behavior of steel structural system and are used to better explain the response of the presented cases hereafter.

ABAQUS provides the means to include the creep strains into the FE models through the incorporation of user-defined subroutine (CREEP). The subroutine is developed as per ABAQUS documentation (*ABAQUS ver. 6.14 documentation* 2014) and based on Fields and Fields (1989) constitutive creep model, taking into account unit consistency. The development of the subroutine is explained in the next chapter.

CHAPTER III

DEVELOPMENT OF THE METHODOLOGY

This chapter describes the proposed methodology for explicit modeling of the thermal creep of steel under transient-state temperature environment of structural fires. Specifically, a procedure is developed and implemented as user-defined subroutines in ABAQUS structural-fire applications.

A. Formulation of thermal creep of steel

In order to develop a procedure to explicitly account for the creep of structural steel under changing temperature environment of a building fire, a computational material creep model is formulated. The constitutive creep material law in the form of power-law by Fields and Fields (1989) is utilized in the formulation of the computational model and its implementation as a user-defined subroutine (CREEP) in ABAQUS. The proposed model by Fields and Fields (1989) was developed for the ASTM A36 steel, which is chemically similar to S275 steel, in the temperature range of 350 °C to 600 °C, and for creep strains up to 6 %. As discussed before, this model includes only the primary and secondary stages of creep (Fig. 2). The empirical equation proposed by Fields and Fields (1989) in the form of power-law (Norton-Bailey) equation is shown in Eq. (6).

$$\varepsilon_c = at^b \sigma^c \quad (6)$$

In Eq. (6), the coefficients a , b , and c are positive temperature-dependent material constants. Formulas for the calculation of these material constants are presented in Eqs. (7), (8) and (9).

$$b(T) = b_0 + b_1 T \quad (7)$$

where $b_0 = -1.1$ and $b_1 = 0.0035$

$$c(T) = c_0 + c_1 T \quad (8)$$

where $c_0 = 2.1$ and $c_1 = 0.0064$

$$a(T) = (0.145^c) 10^{-(a_0 + a_1 T)} \quad (9)$$

where for $T < 500^\circ\text{C}$, $a_0 = 8.1$ and $a_1 = 0.00573$, and for $T > 500^\circ\text{C}$, $a_0 = 15.25$ and

$a_1 = -0.00851$. In Eqs. (7), (8), and (9), T is in $^\circ\text{C}$, t is in minute, σ is in MPa, and ε_c

is in mm/mm (unitless).

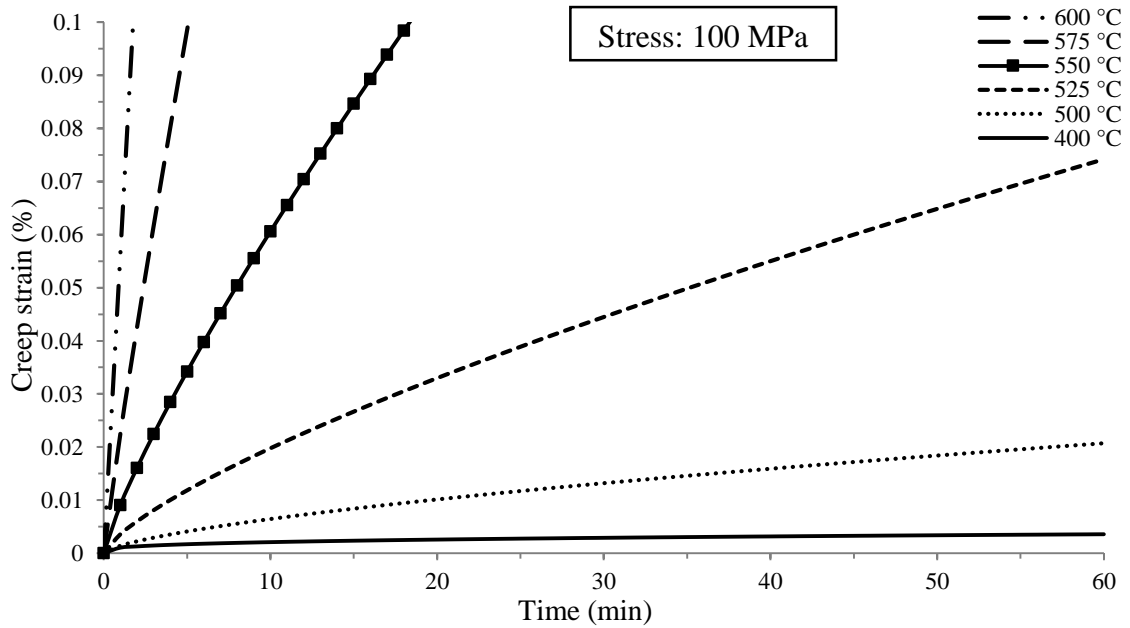


Figure. 2. Fields and Fields creep model of structural steel (1989).

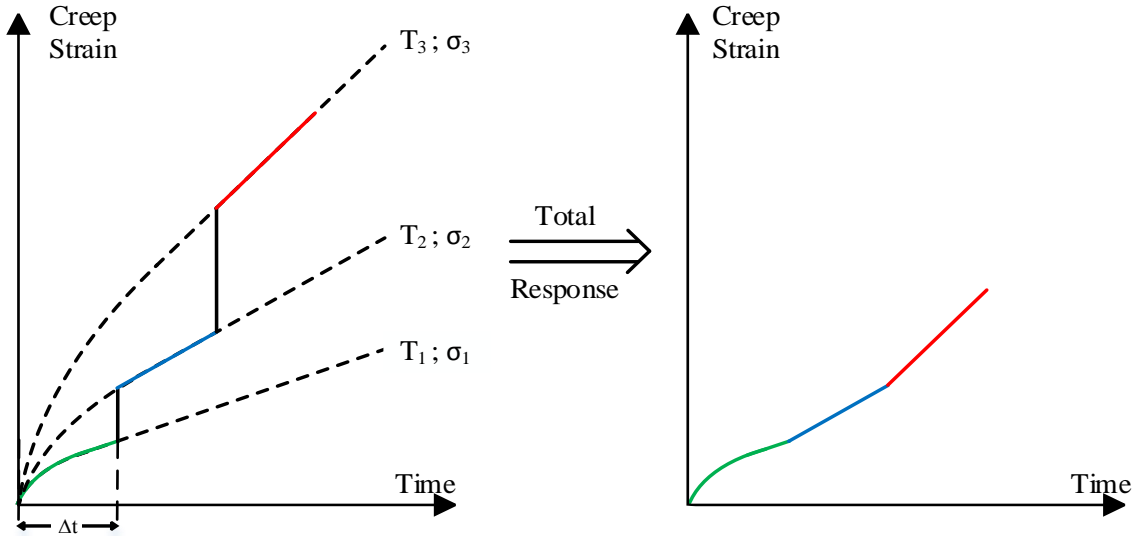
To formulate the computational material model and calculate creep strains, an equation for the creep strain rate is necessary. The creep strain rate can be represented in two different formats: time- and strain-hardening formats. In the time hardening formulation, the creep strain rate is defined as a function of time, as shown in Eq. (10).

$$\dot{\varepsilon}_c = F(t; \sigma; T) = abt^{b-1} \sigma^c \quad (10)$$

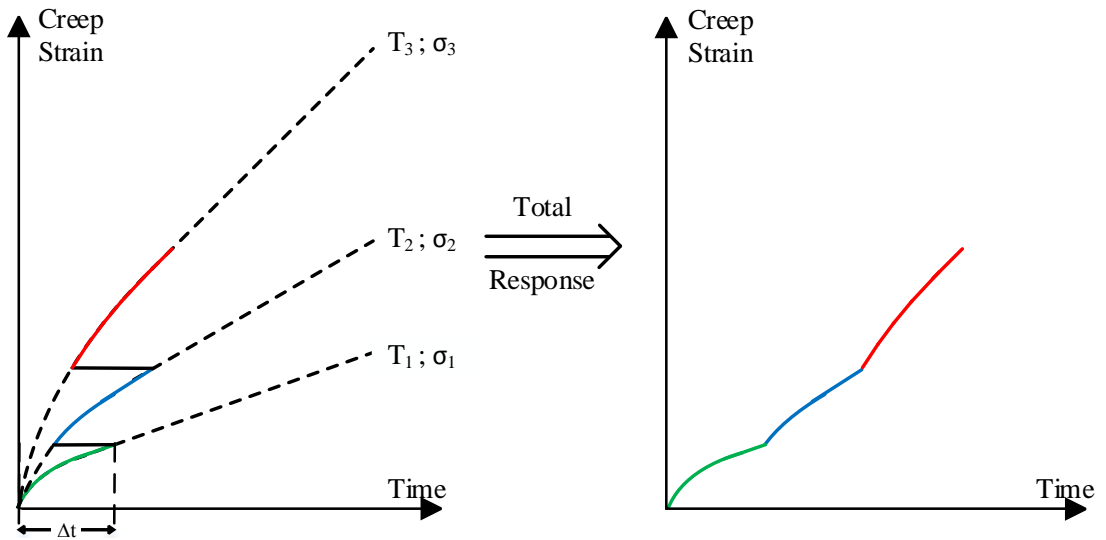
Whereas in the strain hardening formulation, the creep strain rate is defined as a function of the creep strain, as shown in Eq. (11). Figure 3 further depicts these two representations in numerical integration forms.

$$\dot{\varepsilon}_c = F(\varepsilon_c; \sigma; T) = a^{\frac{1}{b}} b \varepsilon_c^{\frac{b-1}{b}} \sigma^{\frac{c}{b}} \quad (11)$$

In Eqs. (10) and (11), $\dot{\varepsilon}_c$ is in per minute. It has been shown in previous studies (Kodur & Dwaikat 2010; Morovat 2014) and confirmed in this study that the strain hardening formulation yields better and more accurate results when computing the time-dependent strains for variable stress history. Therefore, in this study, the Fields and Fields (1989) equation is described in a strain-hardening formulation.



(a)



(b)

Figure. 3. Creep response when changing stress or/and temperature (a) using time hardening formulation; (b) using strain hardening formulation.

Equation (11) can be further simplified, through the change of the constants (a , b , and c), as shown in Eq. (12):

$$\dot{\epsilon}_c = \left[A \sigma^n (\epsilon_c (m+1))^m \right]^{\frac{1}{m+1}} \quad (12)$$

where $A = ab$, $m = b-1$, and $n = c$

The creep strain difference per iteration can be written as follows:

$$\Delta \varepsilon_c = \left[\left(\frac{A\sigma^n}{1+m} \right)^{\frac{1}{1+m}} \times \Delta t + \varepsilon_c^{\frac{1}{1+m}} \right]^{1+m} - \varepsilon_c \quad (13)$$

In case of implicit integration, the derivative of the strain difference with respect to the equivalent stress needs to be included in the subroutine as per ABAQUS documentation (*ABAQUS ver. 6.14 documentation 2014*) and can be written as follows:

$$\frac{\partial \Delta \varepsilon_c}{\partial \sigma} = \frac{\Delta t n}{\sigma} \left(\frac{A\sigma^n}{m+1} \right)^{\frac{1}{m+1}} \left[\Delta t \left(\frac{A\sigma^n}{m+1} \right)^{\frac{1}{m+1}} + \varepsilon_c^{\frac{1}{1+m}} \right]^m \quad (14)$$

Note that it is more convenient to use implicit integration scheme since it is unconditionally stable. However, a tolerance is assigned to reach accurate results by controlling the difference in the change of creep strain between the iterative steps ($\Delta \varepsilon_{i+1} - \Delta \varepsilon_i < tolerance$). If the difference is not within the predefined tolerance, the iteration is repeated with a smaller Δt until the tolerance is satisfied.

As mentioned before, the creep models available in literature describe creep behavior by an equivalent uniaxial behavior. That is, in three-dimensional (3D) space, stress is applied at one direction and the other two directions are assumed stress-free. However, in 3D FE models of steel frames, such conditions are unlikely to happen; normal and shear stresses can exist at the three directions at the same time (multi-axial stresses). In ABAQUS, the creep strains are computed based on the von Mises, also called equivalent, stress (σ_v).

$$\sigma_v = \sqrt{\frac{1}{2} \left[(\sigma_{xx} - \sigma_{yy})^2 + (\sigma_{yy} - \sigma_{zz})^2 + (\sigma_{zz} - \sigma_{xx})^2 \right] + 3(\tau_{xy}^2 + \tau_{yz}^2 + \tau_{zx}^2)} \quad (15)$$

The corresponding equivalent, von Mises, strain (ε_v) can be expressed as:

$$\sigma_v = E\varepsilon_v \quad (16)$$

Based on Hook's law, the relationship between stress and strain vectors is as follows:

$$\begin{bmatrix} \sigma_{xx} \\ \sigma_{yy} \\ \sigma_{zz} \\ \tau_{xy} \\ \tau_{yz} \\ \tau_{zx} \end{bmatrix} = \begin{bmatrix} \lambda + 2G & 0 & 0 & 0 & 0 & 0 \\ 0 & \lambda + 2G & 0 & 0 & 0 & 0 \\ 0 & 0 & \lambda + 2G & 0 & 0 & 0 \\ 0 & 0 & 0 & G & 0 & 0 \\ 0 & 0 & 0 & 0 & G & 0 \\ 0 & 0 & 0 & 0 & 0 & G \end{bmatrix} \begin{bmatrix} \varepsilon_{xx} \\ \varepsilon_{yy} \\ \varepsilon_{zz} \\ \gamma_{xy} \\ \gamma_{yz} \\ \gamma_{zx} \end{bmatrix} \quad (17)$$

where:

$$\lambda = \frac{\nu E}{(1+\nu)(1-2\nu)} \quad (18)$$

$$G = \frac{E}{2(1+\nu)} \quad (19)$$

Combining Eqs. (15), (16), and (17) yields:

$$\varepsilon_v = \frac{1}{\sqrt{2(1+\nu)}} \sqrt{(\varepsilon_{xx} - \varepsilon_{yy})^2 + (\varepsilon_{yy} - \varepsilon_{zz})^2 + (\varepsilon_{zz} - \varepsilon_{xx})^2 + \frac{3}{2}(\gamma_{xy}^2 + \gamma_{yz}^2 + \gamma_{zx}^2)} \quad (20)$$

Creep strains are considered to follow the same deformation mechanism as that of the plastic strains. That is, no volumetric change is caused by the creep deformations (plastic *Poisson's* ratio: $\nu_p = 0.5$), regardless of the assigned material *Poisson's* ratio.

This implies the following distribution of the creep strains:

$$\begin{bmatrix} \Delta\varepsilon_{c,xx} \\ \Delta\varepsilon_{c,yy} \\ \Delta\varepsilon_{c,zz} \\ \Delta\varepsilon_{c,xy} \\ \Delta\varepsilon_{c,yz} \\ \Delta\varepsilon_{c,zx} \end{bmatrix} = \left(\frac{\Delta\varepsilon_c}{2(1+\nu)\varepsilon_v} \right) \begin{bmatrix} 2 & -1 & -1 & 0 & 0 & 0 \\ -1 & 2 & -1 & 0 & 0 & 0 \\ -1 & -1 & 2 & 0 & 0 & 0 \\ 0 & 0 & 0 & 3 & 0 & 0 \\ 0 & 0 & 0 & 0 & 3 & 0 \\ 0 & 0 & 0 & 0 & 0 & 3 \end{bmatrix} \begin{bmatrix} \varepsilon_{xx} \\ \varepsilon_{yy} \\ \varepsilon_{zz} \\ \gamma_{xy} \\ \gamma_{yz} \\ \gamma_{zx} \end{bmatrix} \quad (21)$$

B. Temperature environments

Based on the presented equations, user-defined subroutines are developed to consider different temperature environments which are thoroughly explained in this section.

1. Steady-state temperature environment

In steady-state analysis, both the temperature and the load applied are held constant. Such conditions are mainly provided in material creep tests to directly measure the strains with respect to time. To better understand the time-dependent behavior of steel structures under elevated temperature without the interference of any other parameter, the steady-state analysis is chosen to be the first stage of this study. The coefficients (A , m , and n) associated with the subroutine are solely dependent on the instant temperature of steel, which is maintained constant at this stage. Therefore, these coefficients remain constant throughout the simulation, and thus can be manually calculated and introduced in the subroutine when developing the FE model. To account for the expected change in the element stresses due to different reasons (e.g. stress relaxation, geometrical nonlinearity...) during the FE analysis, the strain hardening formulation is utilized in the subroutine. An example of the developed steady-state subroutines can be found in the Appendix section.

2. Stepwise steady-state temperature environment

As a first step towards studying the behavior of the system under transient-state heating, a consecutive steady-state *creep* steps are conducted while including the creep material. This method is done by assigning a heating step, where temperature is increased

by constant increments without the creep effect, followed by a steady-state *creep* step for a specific duration. This procedure is repeated, in a step-by-step manner, until reaching the desired temperature. The smaller the size of steps is, the more accurate the results will be. Since only one user-defined subroutine can be assigned to a single FE simulation (job) in ABAQUS, the subroutine created for this stage includes conditional statements which control the coefficients that should be used depending on the temperature reached in each step. The subroutine used for the stepwise steady-state analyses can be found in the Appendix section.

3. Transient-state temperature environment

In real fire scenarios, a transient-state conditions are more likely to occur than steady-state conditions. Therefore, it is essential to carry out numerical studies on steel structures subjected to temperature change while including the time-dependent effect especially when reaching high temperatures (above 400 °C). Transient-state analysis is defined when both temperatures and stresses are considered as variables. As mentioned before, the change in stress is taken into consideration by using the strain hardening formulation as a criterion. However, the change in temperature implies that the three temperature-dependent coefficients (A , m , and n) also vary with time. Therefore, the subroutine is modified so that it can perform transient-state analysis within a single analysis step. The equations of temperature-dependent coefficients are included in the subroutine. This modification enables automated computation of these coefficients at the beginning of each incremental step based on the new temperature. To inhibit the formation of any creep strains below 350 °C, A is set to zero for all temperatures below this temperature. A summary of the subroutine calculation process is illustrated as a

flowchart in Fig. 4. In numerical solutions, such as FE analysis, time is discretized into increments where each increment is treated under steady-state conditions (temperature, stress ...). That is, in numerical solutions, the transient-state analysis is basically a chain of steady-state increments linked together. The same applies to how the subroutine works (*ABAQUS ver. 6.14 documentation 2014*), in incremental steps, at each iteration the temperature and stress are assumed constant during the increment. At the start of each increment, and that is what the flowchart is representing, the subroutine is called to estimate the change in creep strain [Eq. (13)] based on the instant stress, temperature, and creep strain history of each mesh element in the FE model. The conditions are assumed constant throughout the increment.

It is noted that implicit and explicit integration schemes follow the backward and forward Euler integration methods, respectively. Thus, the temperature used in calculating the temperature-dependent coefficients is the temperature at the end of each increment for implicit integration scheme and vice versa. However, this difference in the outcome can be hardly noticed if the increment is very small, where the difference between the beginning and the end temperature is almost negligible. Note that only the implicit integration scheme is used in this study for all the cases hereafter.

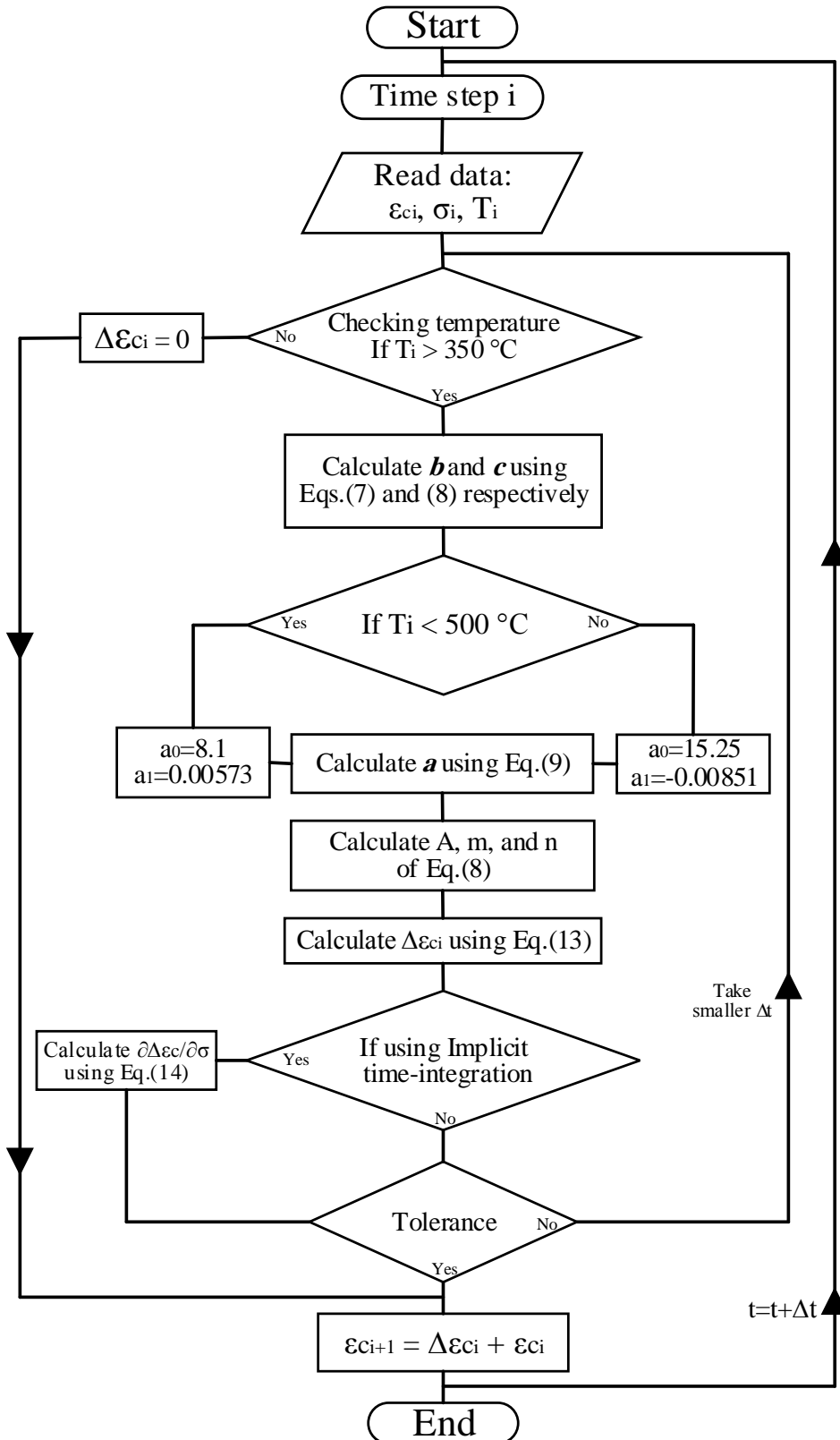
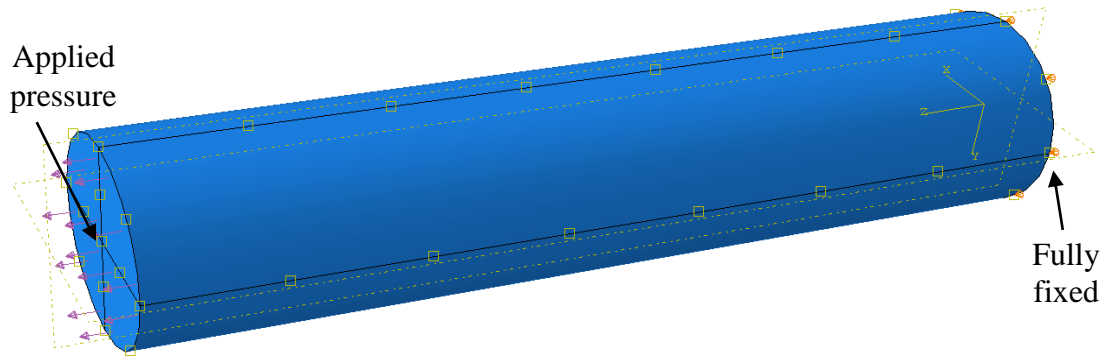


Figure. 4. Flowchart representing the subroutine incremental solution.

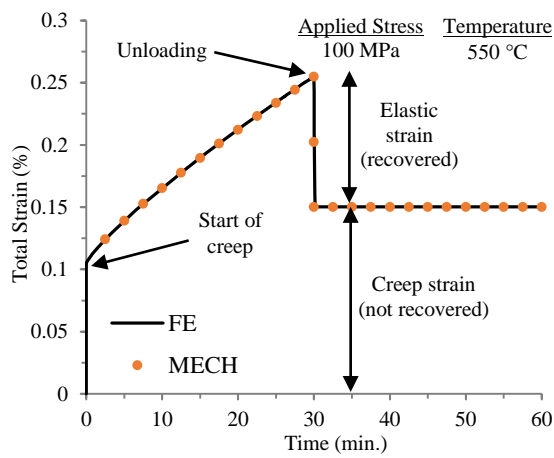
C. Testing the subroutine

Many trials on simple FE models are done to ensure that the developed subroutine is functioning well before applying it to complex models as the ones established in this study hereafter. An example is illustrated in Fig. 5, and it focuses on the issue of stress removal and stress reversal. The stress variation is an important aspect in the development of creep strains. The example consists of a cylindrical shape steel element at temperature of 550 °C under uniaxial constant stress (100 MPa). Then, after 30 min, a sudden removal of stress occurred and, as can be seen from Fig. 5(b), only the elastic strain is recovered, which is in confirmation with the expected behavior. The creep strains are, as stated in the introduction, time-dependent inelastic (plastic) strains, and they are treated as such (irreversible strains) in ABAQUS models.

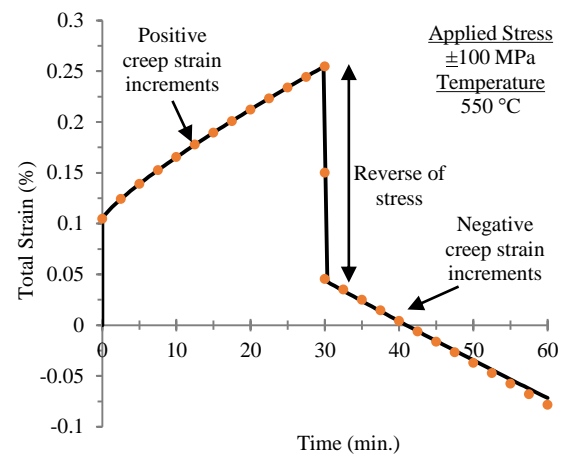
Despite the fact that Fields and Fields (1989) creep model is empirical in nature and, mathematically, negative stresses cannot be input to the original equation [Eq. (6)], the subroutine algorithm can check for negative stresses. Thus, negative stresses yield negative creep strains increments and vice versa. That is clearly proven in the second scenario [Fig. 5(c)]. More detailed explanation of the subroutine algorithm functionality can be found in ABAQUS documentation (*ABAQUS ver. 6.14 documentation* 2014). Due to its simplicity (uniaxial stress case), this example can be represented by a mechanical-based *Maxwell* model (Fig. 6) which consists of a spring and a dashpot in series. The spring represents the linear elastic deformations (since the applied stress is less than the yielding stress) and the dashpot represents the time-dependent (creep) irreversible deformations. To include the primary and secondary stages of creep, a nonlinear dashpot is assigned which follows the used creep model (Fields & Fields 1989). The results show a perfect agreement between the mechanical and FE predictions [Fig. 5(b) and (c)].



(a)



(b)



(c)

Figure. 5. FE vs. mechanical model results: (a) trial model used to test the subroutine; (b) unloading scenario; (c) reverse loading scenario.

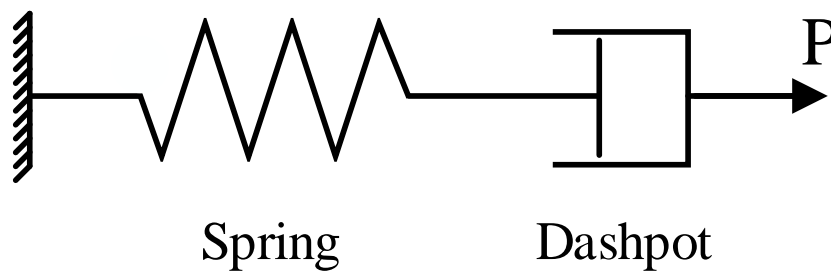


Figure. 6. Maxwell model.

CHAPTER IV

FE MODELING OF SHEAR TAB CONNECTION ASSEMBLY

A total of ten fire tests were carried out by Wang et al. (2011) to study the effect of column size (level of axial restraint) on different types of connections. Only two of these tests were conducted to investigate the behavior of shear tab connections of steel sub-frames (Tests 1 and 6) that will be used in the study. FE models of the two shear tab connection assemblies are developed in ABAQUS to reproduce the same geometrical and material properties reported in the experiment. The assembly details are shown in Fig. 7, and a summary of the component properties are presented in Table 1. The results obtained from the FE models are then evaluated against that from the corresponding experiment. A description of the structural components, the analysis procedure conducted in the FE models, and the observations cited during the simulations are presented in the following sections.

Table 1. Summary of the frame assembly components properties.

Test No.	Frame Components	Section/Dimension	Material Grade
Test 1	Column	UC 254 × 254 × 73	S355
	Beam	UB 178 × 102 × 19	S275
	Shear tab plate	PL 150 × 130 × 10	S275
	Bolts	Four M20 bolts	G8.8
Test 6	Column	UC 152 × 152 × 23	S275
	Beam	UB 178 × 102 × 19	S275
	Shear tab plate	PL 150 × 130 × 10	S275
	Bolts	Four M20 bolts	G8.8

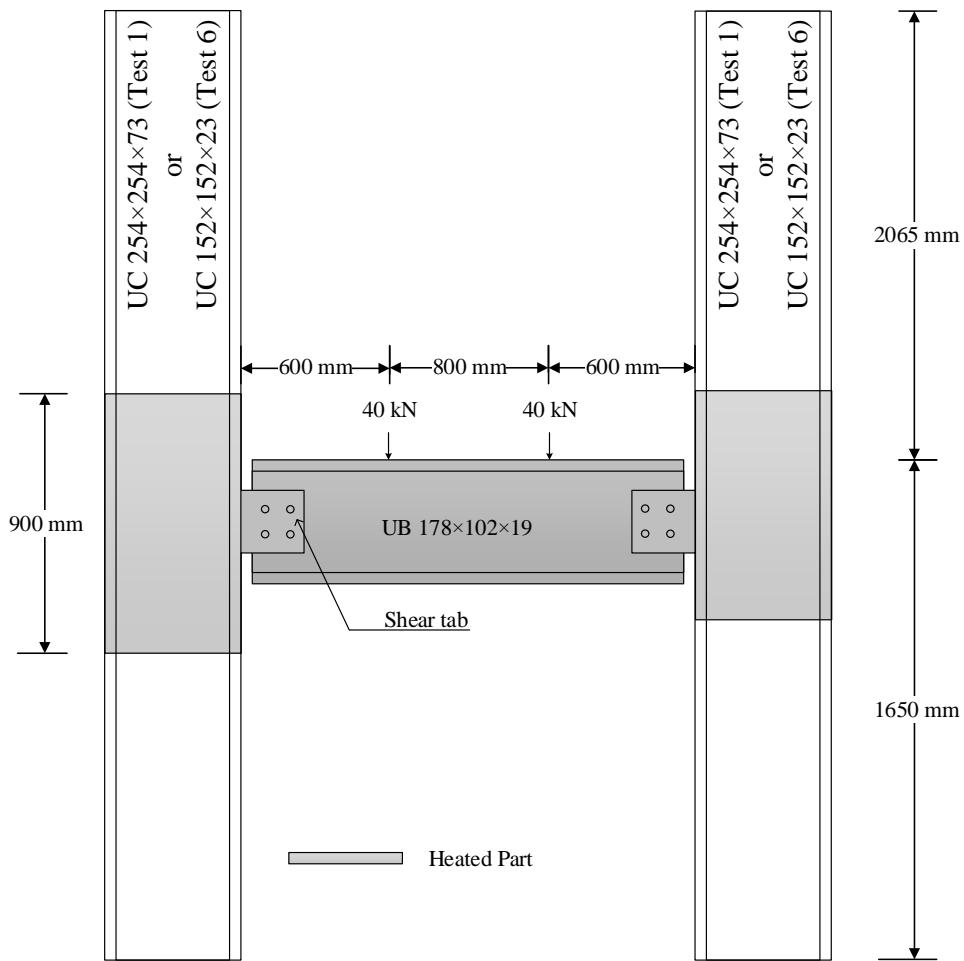


Figure. 7. Details on the fire tests steel frames assembly of Wang et al. (2011).

A. Development of the FE models

1. Geometry of the structural components

The shear tab connection assembly used in the analyses consists of one steel plate $150 \times 130 \times 10$ mm which connects a UB $178 \times 102 \times 19$ beam to the column. Two different column sections are used: UC $254 \times 245 \times 73$ for Test 1 and UC $152 \times 152 \times 23$ for Test 6 (the same notation will be used for both cases hereafter). The plate is welded to the column while bolted to the beam. Four shear bolts of diameter 20 mm (M20) are used with bolt holes of diameter 22 mm (standard size holes). The details of the shear tab connection are shown in Fig. 8.

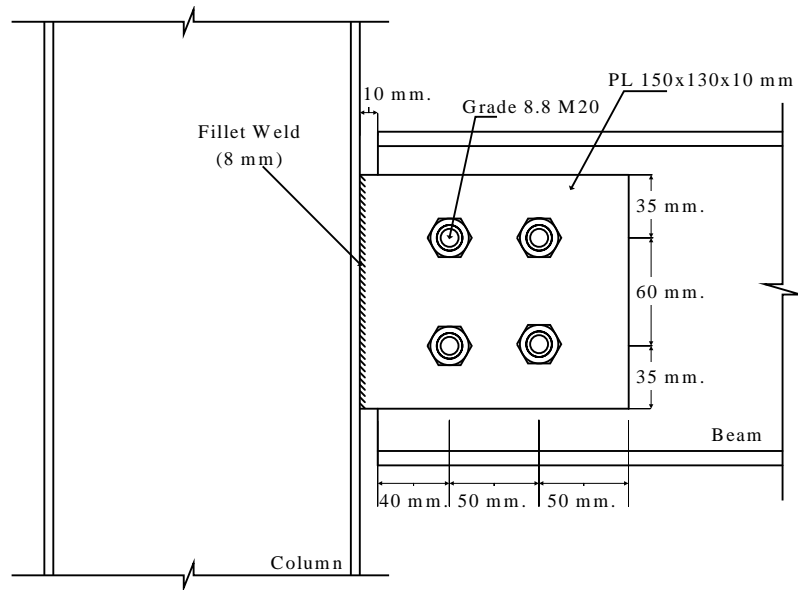


Figure. 8. Details of the shear tab connection.

2. Material properties

An idealized bilinear model is used for the steel materials to incorporate the isotropic hardening of steel with von Mises yielding criterion. The ambient material properties used for the structural parts in the FE models are in agreement with the material properties reported in the experiment. The shear tab plate and the beam are grade S275 steel, yet tensile coupon tests were performed, in the experiment, at ambient temperature and the average yield stress of the tensile coupons taken from the tested beams was found to be 345 N/mm^2 . The UC $254 \times 245 \times 73$ (Test 1) and UC $152 \times 152 \times 23$ (Test 6) columns are of Grade S355 and S275 steel, respectively. The shear tab bolts and nuts are of Grade 8.8. For all the steel components, *Poisson's* ratio is taken as 0.3, and it is assumed to be temperature-independent of steel.

For the estimation of the mechanical properties of steel at elevated temperatures, the creep-free stress-strain-temperature relationship proposed by Lee et al. (2013) are used for the structural steel material, whereas the retention factors proposed by Hu et al.

(2007) are used for the structural bolts. Due to the fast heating (standard fire temperature-time curve) and, creep material is not included in steel properties. Material fracture is not considered in the analyses.

3. Model discretization

All components of the assembly model in ABAQUS are discretized using eight-node brick elements with reduced integration (C3D8-R). The C3D8-R elements are suitable for modeling nonlinear 3D structural problems; it has eight nodes with three degrees of freedom (translation in x, y and z direction) at each node. To account for the high stresses present in the connection region where the failure is likely to occur, a relatively finer mesh is used around the connection region. Moreover, to avoid stress concentration around the bolt holes, a mapped meshing technique is used to discretize bolts and their surrounding areas. The bolt heads, shanks, and nuts are modeled as cylindrical volumes.

Surface-to-surface contact with a finite sliding coefficient is used to reproduce contact surfaces. A friction coefficient of 0.25 is utilized to model friction between the contact surfaces, while allowing separation, sliding, and rotation of the contact surfaces. Tie constraint is used to reproduce the fillet weld connecting the shear tab to the column.

4. Applied loads and boundary conditions

Two distinct loading steps are created, one for the pre-tensioning of the shear bolts and the other for applying the two concentrated loads of 40 kN each. Due to the perfect symmetry of structural assembly, half of the frame is modeled in ABAQUS and symmetry is applied at the beam mid span section to save computational time. In the

experiment, there were difficulties to maintain constant and equal force (40 kN) in the hydraulic jacks. However, in the FE model it is assumed to have a constant force with symmetry applied at the mid-span.

To insure stability between bolted elements, pre-tensioning of the bolts is done before applying load to the beam. It is achieved by applying pressure load on the bolt ends with a force equivalent to the required pre-tensioning force. Furthermore, due to the gap present between bolt shanks and bolt holes, and to avoid any rigid body modes, the bolts are given a temporary translation restraint which is later released at the end of the pre-tensioning stage. In the next step, a concentrated vertical force of 40 kN is applied to the steel beam monotonically. This load corresponds to a loading ratio of 0.5 of the plastic moment capacity of the beam section at ambient temperature. The concentrated force is represented by a pressure load distributed on a small area to avoid stress concentration. After that, the frame is heated while holding the applied load constant. Both column ends are horizontally restrained yet free to expand, due to heating, in the vertical direction. In the FE model, a horizontal restraint is assigned to the beam top flange to simulate the lateral restraint provided by the steel truss in the experiment. Details of the FE model are shown in Fig. 9.

5. Temperature profile

In addition to the steel truss connected to the top of the beam in order to impose horizontal restraint in the experiment, the beam top flange was also wrapped with isolating material to include the heat-sink effect of the concrete slab. The furnace size, as specified, was $3000 \times 1600 \times 900$ mm, hence part of the column was present inside the furnace and exposed to fire temperatures. Moreover, some difficulties were encountered

in maintaining uniform distribution of temperature in the furnace and among the structural components of the frame throughout the test. All these factors imply that it is essential to assign different temperature profiles for the different structural components for the sake of including similar experimental conditions. Therefore, the FE model of the test specimen is divided into six regions, each having a uniform temperature distribution.

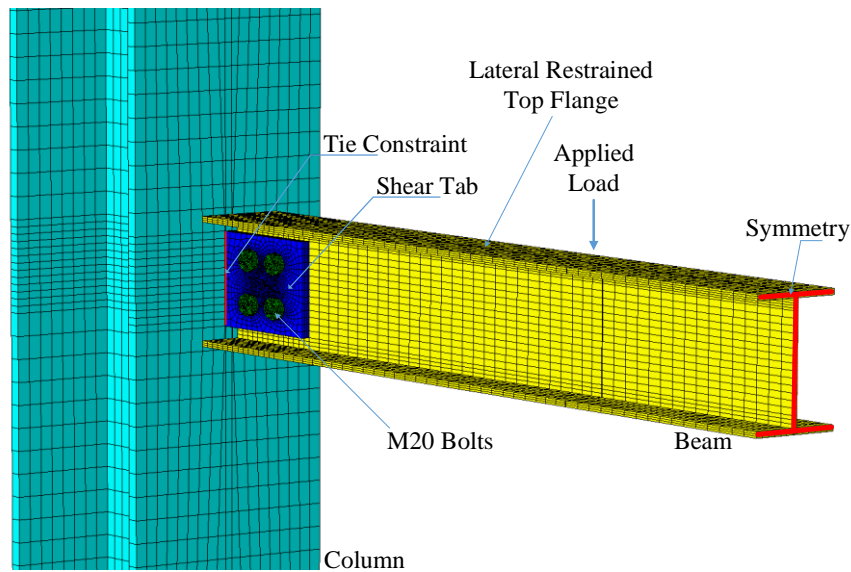


Figure. 9. Detail of the full-scale steel frame FE model assembly.

B. Discussion of the results

Comparison of the FE models' predictions with the experimental results is plotted in Fig. 10. The behavior of the steel frame is represented in terms of the induced beam axial force and the beam mid-span deflection. The case under study is a transient-state heating of an axially restrained beam, therefore the axial force, shown in Fig. 10(a), is developed owing to the restrained expansion of the steel beam. At the beginning of the heating phase, linear increase in the internal beam axial forces and slight increase in the mid-span deflection can be seen, since no significant degradation in the material

properties is present at low temperatures. In Test 1, at about 200 °C, a sudden slip occurs between the shear tab plate and the connected beam web, as shown in Figs. 11(a) and (b), which causes loss in the stored thermal strain energy thus releasing some beam axial stresses. The slip is then followed by bearing of bolt shank [Fig. 11(d)] with the bolt hole [Fig. 11(b)]. The slip is initiated when the axial force in the beam exceeds the statically frictional bond between the plate and the beam web due to the clamping force exerted by the bolts pre-tensioning. No slip is observed in Test 6 since the axial force in the steel beam did not reach high magnitudes. In fact, Test 1 gave higher axial forces due to having stiffer columns than those of Test 6, but mid-span deflection is relatively similar in both cases. Afterwards, a nonlinear increase in axial force and deflection is observed due to material strength and stiffness degradation as temperature increases. As mentioned before, the shear tab connection ductility is mainly due to the ovalization (elongation) of the bolt holes. This is also confirmed in the FE simulations [Fig. 11(c)]. A comparison of the FE models and the corresponding experiment deformed shapes is illustrated in Fig. 12. It can be seen that the FE simulations can predict closely the deformation response of the connection.

Numerical convergence issues are encountered before the start of the cooling (decay) phase. High stresses are observed at the shear tab plate near the vicinity of the weld which indicates a potential weld fracture. The post-ultimate response of the structure cannot be reached in these simulations, since the implicit (ABAQUS/Standard) solver is used to run the simulations without the interference of any stabilizing options or the inclusion of material fracture properties.

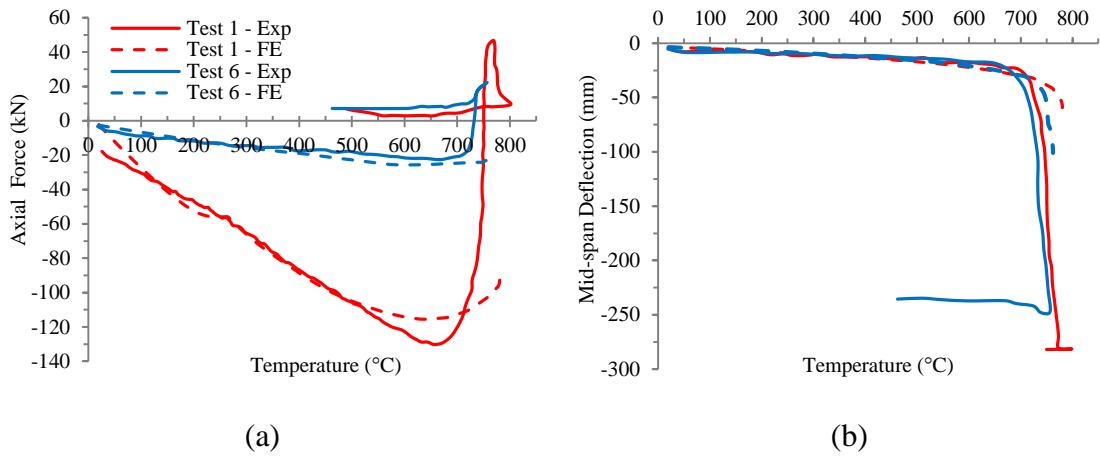


Figure. 10. Comparison between the experimental and FE model results: (a) beam axial force; (b) beam mid-span deflection.

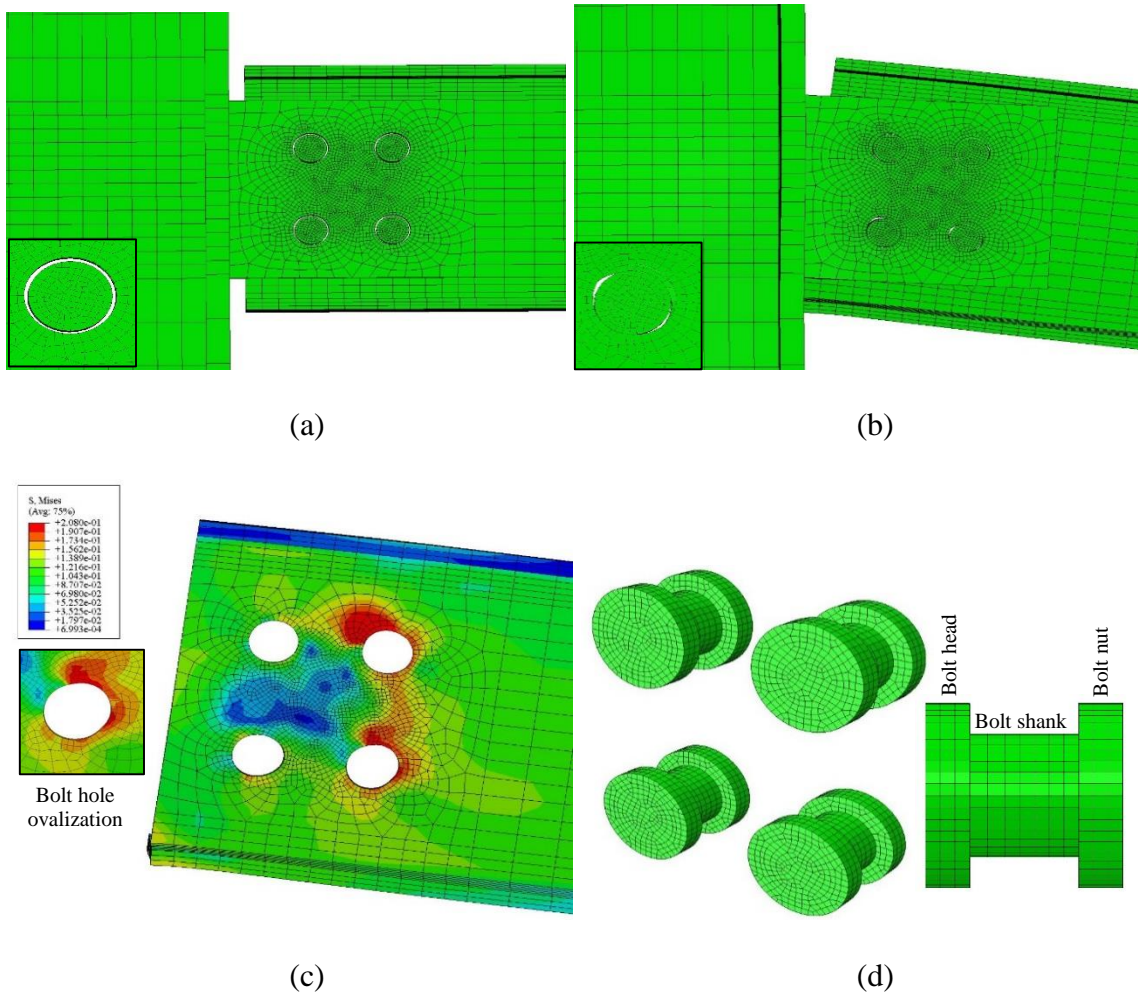
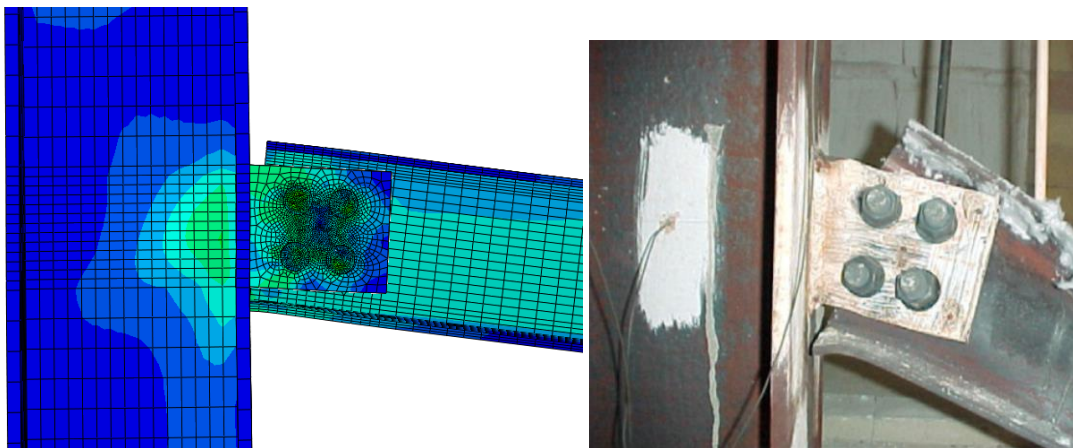
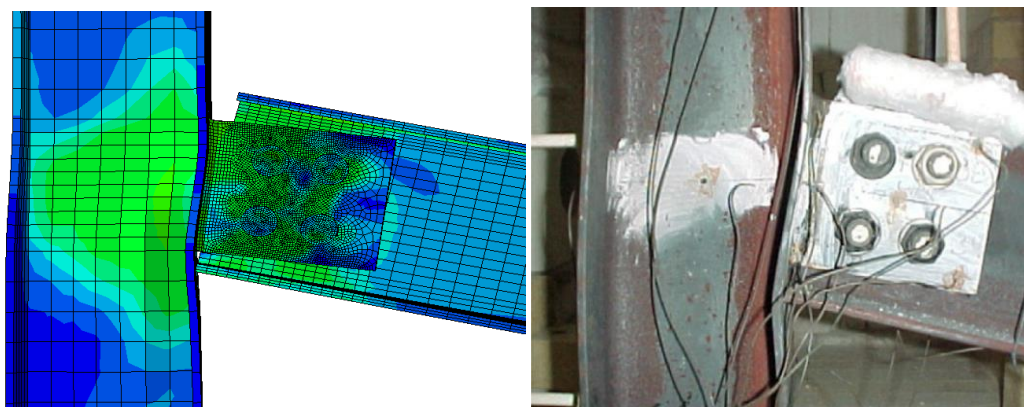


Figure. 11. Shear tab connection behavior: (a) before bolt contact; (b) after bolt contact; (c) bolt hole ovalization (elongation); (d) modeling of shear bolts.



(a)



(b)

Figure. 12. Comparison between FE simulation and experimental (Wang et al. 2011) deformed shapes after the fire test: (a) Test 1; (b) Test 6.

CHAPTER V

EFFECT OF THERMAL CREEP ON THE SHEAR TAB ASSEMBLY RESPONSE

After obtaining the validated scenarios, an extensive parametric study is conducted with some modifications. Unlike the validated conditions, a uniform distribution of temperature is assigned to all the heated structural components for simplicity. In addition, due to the limitations imposed through the application of the creep model by Fields and Fields (1989), the maximum temperature of 600 °C is considered. The developed user-defined subroutine is assigned to both the beam and the shear tab plate. Creep effect is not considered in modeling bolts since they do not contribute much to the overall ductility of the connection, and thereby do not have major impacts on the time-dependent response of the connection. To focus on the beam and connection behavior and to insure a constant end-restrain stiffness for all cases, creep is also not incorporated in the steel column material. The developed user-defined subroutine is activated by changing the analysis step type to *VISCO*. The mesh element type used in the FE analysis (C3D8-R) is capable of incorporating creep strains. Moreover, in contrast to the conventional static (general) FE analysis, defining the time of the analysis step is important when introducing creep effect. During the analysis, the implicit integration scheme is always employed for incorporation of creep strains development, as this method is unconditionally stable and can check for structural equilibrium and stability. A summary of all simulations conducted in this research is presented in Table 2 in the Appendix section. The results of significance are presented in this chapter.

A. Time-dependent simulations: steady-state temperature environment

The model was first heated up to the desired temperature (400 °C, 450 °C, 500 °C, 550 °C, and 600 °C) with load applied and without including creep effect (*very fast* heating rate). The temperature was assumed to increase linearly with time and uniformly distributed in the heated parts of the structure. After the heating step was completed, the final temperature reached was maintained constant and a steady-state *creep* step (*VISCO*) for 120 minutes was then started with creep effect included in the beam and shear tab plate as mentioned before. The constants (A , m , and n), available in Eqs. (13) and (14), were calculated based on the final temperature reached in the heating step and were included in the subroutine. To control the accuracy of the results, a small tolerance of 10^{-6} was assigned.

The variation in the beam axial force and the mid-span deflection during the steady-state temperature simulations are shown in Figs. 13 and 14, respectively. As can be seen, after the steady-state *creep* step is initiated, the beam axial force starts to decrease gradually. During the first few minutes, the primary stage takes place by rapid decrease in the axial force which is then followed by secondary stage associated with slow and steady decrease in the axial force. This decrease in the axial force is due to the stress relaxation caused by the restrained thermal expansion. Similarly, as shown in Fig. 14, the mid-span deflection increases with time during the steady-state temperature step.

For high temperatures (greater than 500 °C), where the creep strain rate is much higher, a severe impact of creep on the behavior of the connection assembly starts to take place. The loss in axial force is observed in a shorter duration. The mid-span deflection also experiences a rapid increase, especially during the first few minutes, caused by the generated moment of the applied load. The degradation in the material properties in terms

of both strength and stiffness along with the development of significant time-dependent plastic strains result in permanent deformations.

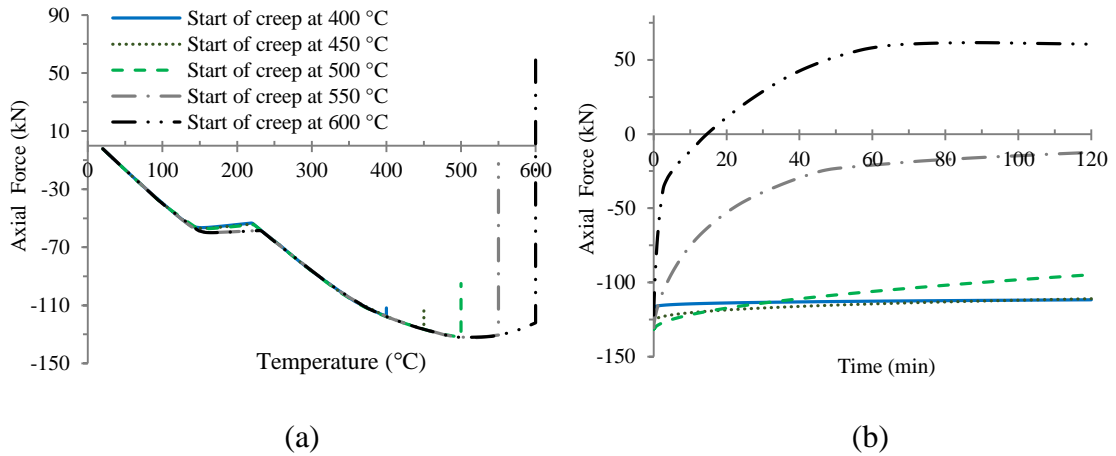


Figure. 13. Beam axial force of steady-state analysis at different temperatures versus (a) temperature; (b) time.

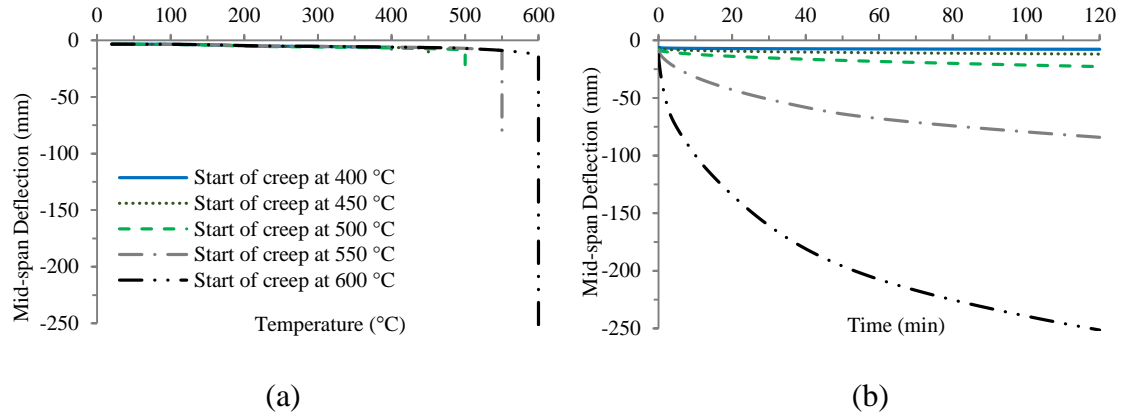


Figure. 14. Beam mid-span deflection of steady-state analysis at different temperatures versus (a) temperature; (b) time.

Based on Eq. (8), c is always greater than unity, meaning that the elastic distribution of stresses will change with time. The nonlinear relation between stress and creep strain rate [Eq. (10)] imposes a redistribution of the stresses over the cross section of the beam. An idealized representation is illustrated in Fig. 15. The FE results (*creep*

starts at 500 °C) of the axial stresses distribution over the beam depth (at the mid-span) versus time, shown in Fig. 16(a), confirm this behavior. At the end of the loading step, the distribution of axial stresses over the beam depth can be seen in Fig. 16(b). After the heating phase takes place, the neutral axis shifts towards the compression zone (downward) as can be seen in Fig. 16(c). In the steady-state *creep* step, the beam is subjected to constant bending moment and additional compression stresses due to restraint thermal expansion. These additional stresses expedite the development of creep strains in the compression zone of the beam section. In response, the beam neutral axis shifts towards the tension zone (downward) to maintain equilibrium. Moreover, at the end of the *creep* step, the redistribution of axial stresses can be seen [Fig. 16(d)] as discussed previously.

Following the mid-span deflection, the connection exhibits excessive rotation because of the loss in the flexural stiffness of the beam through time. Also note that despite the constant temperatures, the stresses are constantly changing due to relaxation. Therefore, the decrease in slope of axial relaxation is caused not only by the transition from primary to secondary stage, but also by the drop in the axial force, which in return results in a decrease in the creep strain rate. Furthermore, at a temperature of 600 °C, the creep effect did not only reduce the compressive stresses but also generated tensile stresses caused by the beam catenary action. The loss of the beam flexural stiffness leads to the resistance of the applied load through alternative equilibrium configuration, namely the catenary action. The presence of beam end axial restraints enables the development of the catenary action to resist the vertical load. Thus, the beam survives for longer durations even after the development of plastic hinges. At a certain point, the tensile forces reach a maximum value, upon which most of the applied load is resisted through

the beam axial stiffness. On the other hand, mid-span deflection continues to increase with a smaller rate.

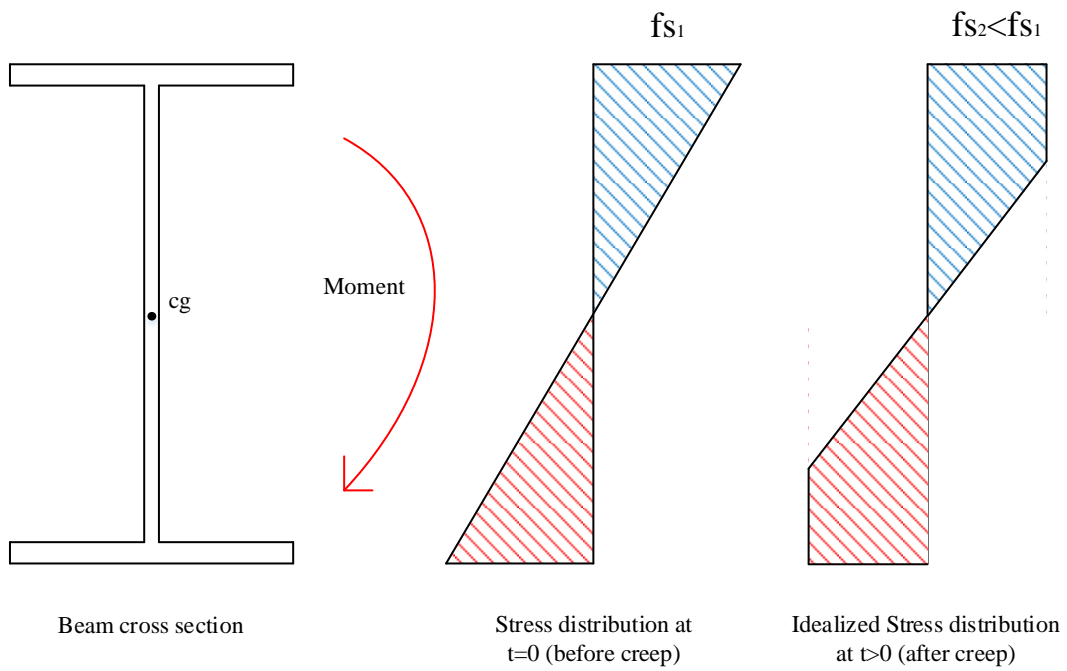
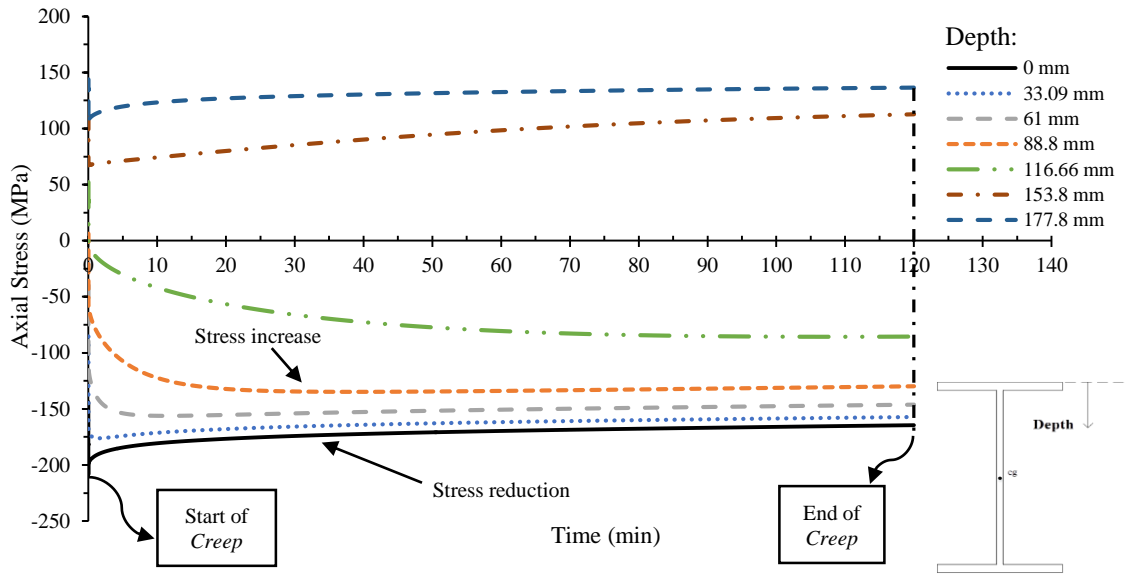
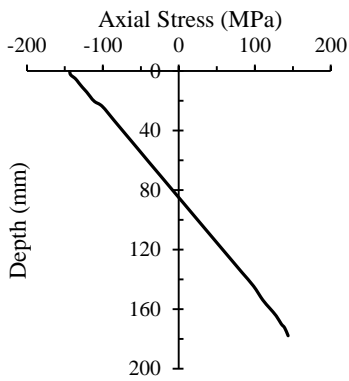


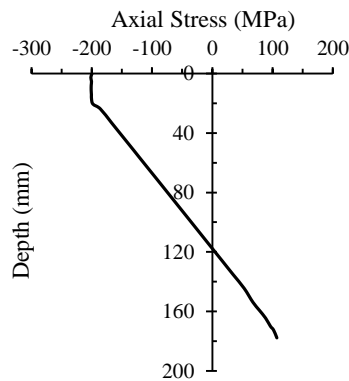
Figure. 15. Axial stress distribution over the cross-section when subjected to constant bending moment, before and after creep.



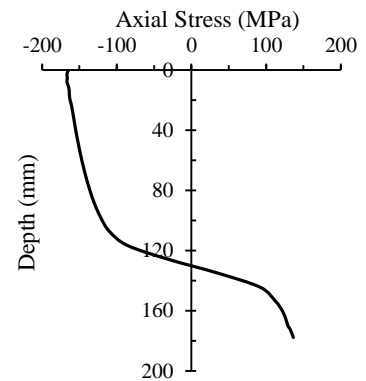
(a)



(b)



(c)



(d)

Figure. 16. Axial stress distribution over the cross-section of the beam at the mid-span (creep starts at 500 °C): (a) at different depths versus time; (b) at the end of loading; (c) at the end of heating; (d) at the end of *creep*.

B. Time-dependent simulations: stepwise steady-state temperature environment

Two *creep* steps durations, both with temperature increase rate of 50 °C/step, are chosen: 5 min/step and 10 min/step which are equivalent to heating rate of 10 °C/min and 5 °C/min, respectively. The resulted beam axial load and the beam mid-span deflection versus temperature are plotted in Figs. 17(a) and (b), respectively. After the load is applied, the temperature is increased from 20 °C to 400 °C, and then consecutive steady-

state *creep* steps are applied as explained previously. It can be seen that the effect of creep is greater for *creep* duration of 10 min/step, and the higher the temperature is the more reduction in compressive stresses is observed. The same can also be applied for the mid-span deflection, which shows a similar behavior. It can be noticed that, according to the adopted creep model by Fields and Fields (1989), the behavior of steel material is highly time-dependent for temperatures above 500 °C. Whereas, for temperatures below 400 °C, creep effect is not significant. The 3D representation of the creep curves (Fields & Fields 1989), illustrated in Fig. 18, explains such response.

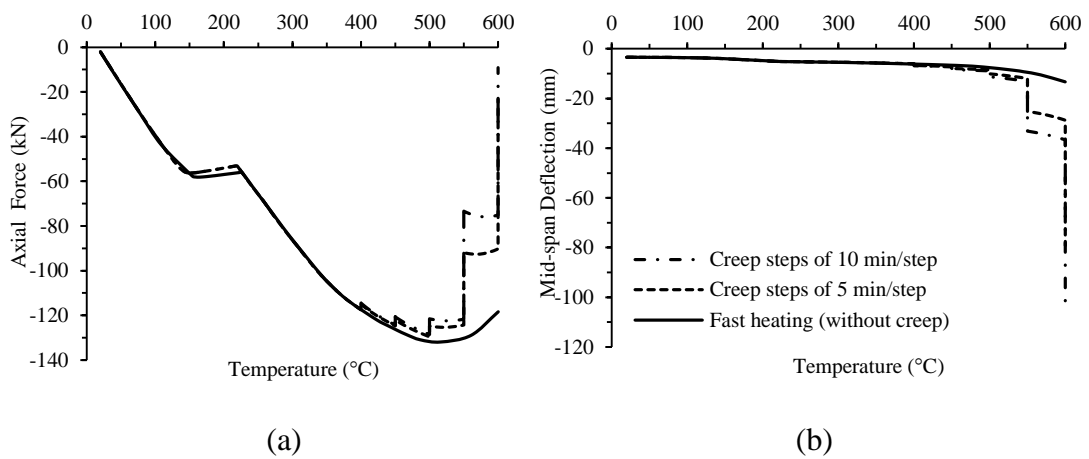


Figure. 17. Stepwise steady-state temperature with and without including creep effect: (a) beam axial force; (b) mid-span deflection.

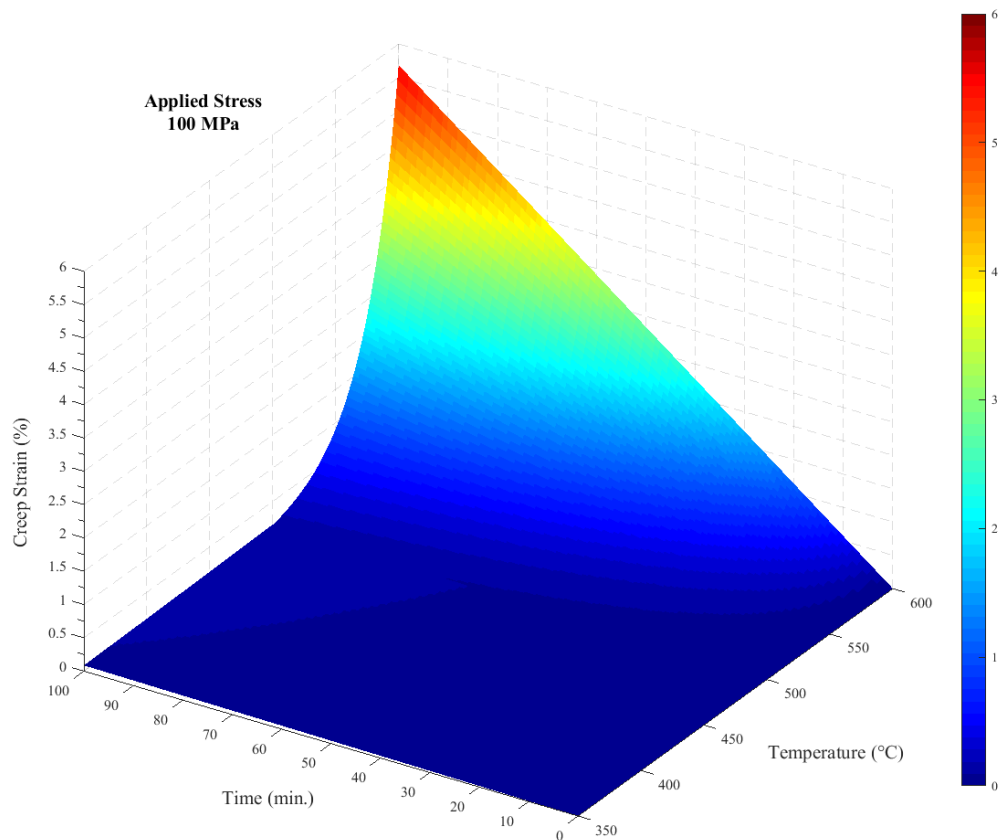


Figure. 18. 3D representation of creep strain-time-temperature curves corresponding to the constant stress of 100 MPa (Fields & Fields 1989).

C. Time-dependent simulations: transient-state temperature environment

Transient-state conditions are applied on the models. The temperature is increased from 20 °C to 600 °C while maintaining the applied load (40 kN). The performance of the steel frame with shear tab connection can be influenced by many factors. These factors can be the geometric configuration of the frame itself or even the fire scenario (temperature-time profile) which the frame is exposed to. Therefore, FE models of the connection assembly are further generated and used to conduct an extensive parametric study of key parameters that affect the time-dependent behavior of the frame during the heating and cooling (decay) phases of fire. These parameters are heating rate, cooling duration, initial cooling temperature, column size, beam geometry, and shear tab

location. FE analysis has proven to be a reliable tool to predict the structural behavior and can reproduce complex geometrical and material nonlinearities. The results obtained from the FE models are compared, discussed, and analyzed to investigate the impact of thermal creep on steel frames with shear tab connections.

1. Parametric studies

The methodology followed in this section is changing a parameter and keeping other parameters constant/unchanged. In that sense, a better understanding can be gained on how each parameter affects the time-dependent behavior of the structural system. Below is an illustration of these parameters with thorough explanation.

a. Heating rate

The fact that creep strains are time-dependent strains entails that heating rate (temperature increase with time) is an important parameter that needs to be investigated. For the case of Test 1, three heating rates are chosen (5, 10, and 20 °C/min) in addition to the case with no creep. Restricted to Fields and Fields (1989) limitations, the maximum temperature reached in the heating phase is 600 °C. The results of the beam axial force and the beam mid-span deflection of Test 1 obtained from ABAQUS are shown in Figs. 19(a) and (b), respectively. At temperatures below 350 °C, no effect of creep can be seen. This returns to the fact that the subroutine is developed based on Fields and Fields (1989) model which considers the temperature 350 °C as a limiting temperature for creep effect to initiate. Afterwards, looking at the beam axial force in Fig. 19(a), the phenomenon of stress relaxation can be clearly seen when introducing the creep effect into the FE models. This is attributed to having the case of restrained beam subjected to temperature increase.

Similar to what discussed in Eq. (5), creep strains result in stress decrease in restrained systems with induced thermal axial stresses. In contrast, creep causes increase in the beam mid-span deflection, as shown in Fig. 19(b), in response to the stresses of the bending moment caused by the constant applied load (40 kN). That is similar to what was discussed in Eq. (4). Moreover, with slow heating rates (e.g. 5 °C/min) the creep effect is more significant: more beam mid-span deflection and more reduction in the axial force can be clearly seen. Nonetheless, the drop in the axial stresses is not entirely caused by stress relaxation phenomenon but also by the geometrical and material nonlinearities, most notably the catenary action of the beam due to the increase in the beam deflection.

Unlike normal conditions, in fire events, there exists an interaction between the beam axial force and the mid-span deflection especially during the late stages of fire. When the beam loses its flexural stiffness due to plastic strains or even creep effect and large deformations occur, the load is transferred through alternative axial path that can maintain equilibrium, slow down beam deflection, and extend the beam survival time. The beam resistance mechanism changes from flexural to axial mechanism, well known as catenary action. This generates, if enough tying capacity exists in the connections, tensile forces in the beam which counteract the thermal compressive forces leading to a decrease in the axial stresses as shown in Fig. 19(a). The catenary action is mainly dependent on the beam material and geometry, applied vertical load and the beam end axial stiffness restraint, represented by the column flexural stiffness.

Based on Fields and Fields (1989) model, the creep strain rate increases exponentially as temperature increases, especially for temperatures higher than 500 °C. That is what explains the fast drop in axial force and fast increase in the mid-span

deflection at high temperatures (above 500 °C). Furthermore, excessive elongation of the bolt holes is observed due to high stresses at the connection region.

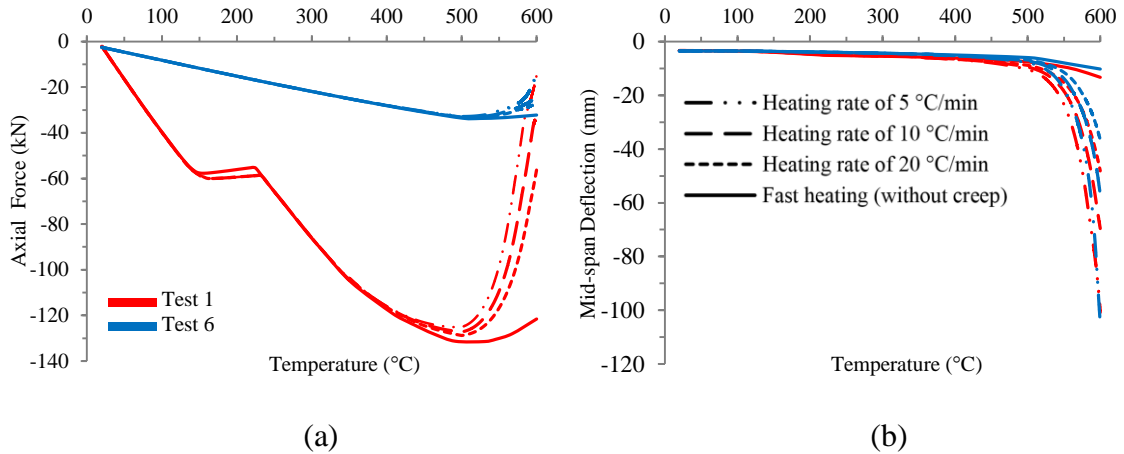


Figure. 19. Results obtained from ABAQUS of different heating rates for Tests 1 and 6: (a) beam axial force; (b) beam mid-span deflection.

b. Column size

The column size has a great impact on the response of the steel frame during fire. In addition to supporting gravity loads, columns also provide an axial restraint at the beam ends through its flexural stiffness. The column flexural stiffness is determined by its length, size (cross section), boundary conditions, and steel material properties. The two column sections of Tests 1 and 6 are used to represent different beam end restraint stiffnesses. FE models of the two column sizes are further generated with different heating rates to understand the effect of beam end restraint stiffness on the development of creep strains. The results of the beam axial force and the mid-span deflection of the two cases are presented in Figs. 19(a) and (b), respectively. It is evident that the column size can greatly influence the development of creep strains. The fact that the stress is a controlling factor of creep strain development [Eq. (10)], the high axial stresses in Test 1 expedite the development of creep strains, unlike Test 6. This is not the case for beam mid-span

deflection where the results are relatively similar in both cases since they have the same applied load (40 kN) with rotationally flexible connection (shear tab connection). Nonetheless, Test 1 is seen to have slightly higher mid-span deflection when compared to Test 6. This is due to the P- Δ effect, where P is the induced axial force on the beam ends and Δ is the vertical deflection. The connection rotation shows similar trend as the beam mid-span deflection as shown in Fig. 20.

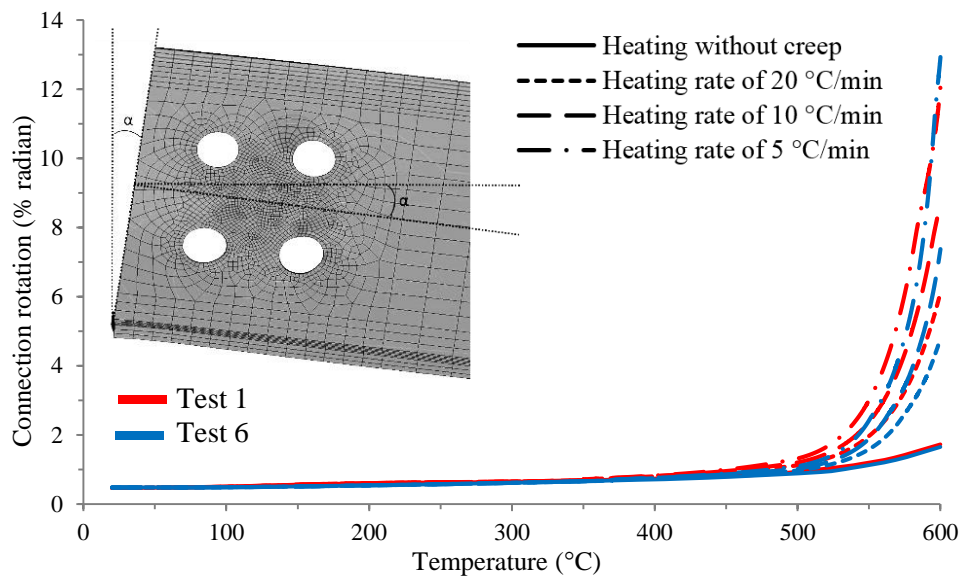


Figure. 20. Connection rotation results for different heating rates.

c. Cooling duration

In the decay phase of fire, the temperature drops back to the ambient/room temperature (20 °C). The duration of which the steel temperature needs to reach back to the ambient temperature is called cooling duration. It is worth mentioning that, in the incremental step of solving, the heating or cooling phases of fire do not directly contribute to the subroutine output since, as mentioned previously, the input temperature is the instant temperature and not the change (variation) in temperature (unlike thermal

expansion) of steel at a given increment. Moreover, temperature does not control the sign (negative or positive increments) of the creep strain, it is rather a factor of initiation of creep effect and one of the factors that control the rate of creep strain development.

Due to the lack of information about the material properties of steel (bolts, base material ...etc.) after exposure to fire temperatures, it is assumed that all the assembly components regain their full strength and stiffness when cooled down to the ambient temperature. The subroutine is also incorporated in the cooling phase since cooling starts from high temperatures, where the creep effect is significant, and drops down to room temperature. Therefore, the response of the connection assembly in the cooling (decay) phase of fire is also considered through applying various cooling durations. Beside the case with no creep, three cooling durations are considered (5, 10, and 20 min). Fig. 21 shows the beam axial force and mid-span deflection for different cooling durations after two heating cases: fast heating (without creep) and heating rate of 20 °C/min. It can be seen that a slow heating rate produces large axial tensile forces at the end of the cooling phase. This can be attributed to the additional loss of the induced beam axial force, during the heating phase, due to the development of creep strains at slower heating rates. For faster heating rates, the difference between the results of the four cooling durations can be clearly seen since the compression axial force at the end of the heating phase is larger, causing faster creep rate. When the tension force reaches almost the same magnitude (about 60 kN) at which the first slip occurred (during the heating phase), a reverse slip is observed during the cooling phase.

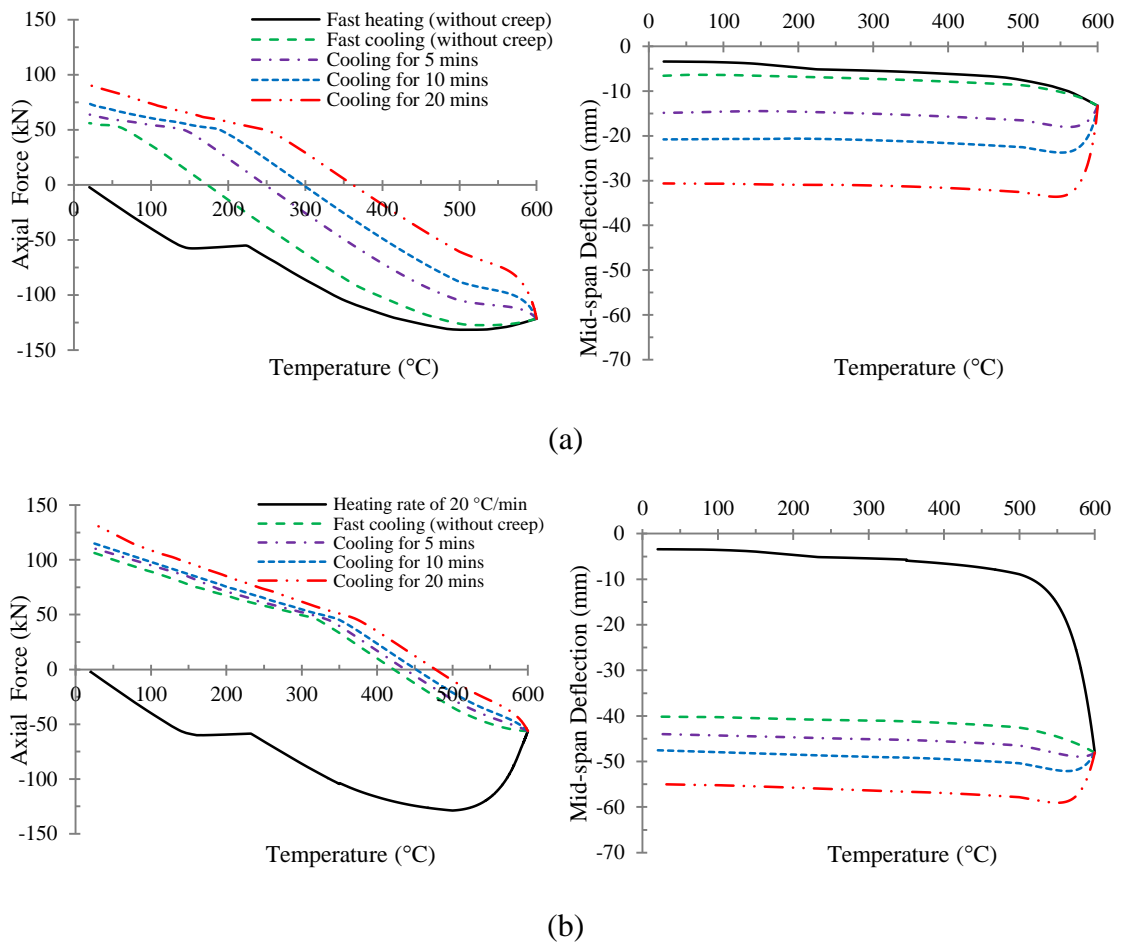


Figure. 21. Beam axial force and mid-span deflection response for different cooling durations after: (a) fast heating (without creep); (b) heating rate of 20 °C/min.

d. Initial cooling temperature

It was observed by many researches that failure of the connections occurs mostly during the decay phase of fire (Selamet & Garlock 2010) due to the generated tensile forces. Insufficient tying force capacity of steel connections can lead to failure of these connections, and, consequently, the failure of the whole system. Depending on the fire scenario of which the frame is exposed to or whether the steel member is protected or not, the maximum steel temperature reached in the heating phase of fire can change from a case to another. This is denoted as the initial cooling temperature. The initial cooling temperature can greatly affect the response of the system at the end of the cooling phase.

Results of three different initial cooling temperatures (500 °C, 550 °C, and 600 °C), following the same heating rate (20 °C/min), are presented in Fig. 22. It can be clearly seen that as the initial cooling temperature increases, the beam tensile force and mid-span deflection at the end of the cooling phase increase. This is caused by the loss of compressive forces at high temperatures due to creep and catenary action, which results in increased tensile stresses at the cooling phase. Since it is assumed that the steel material regains its full strength after cooling, as mentioned before, no failure in the connection is observed.

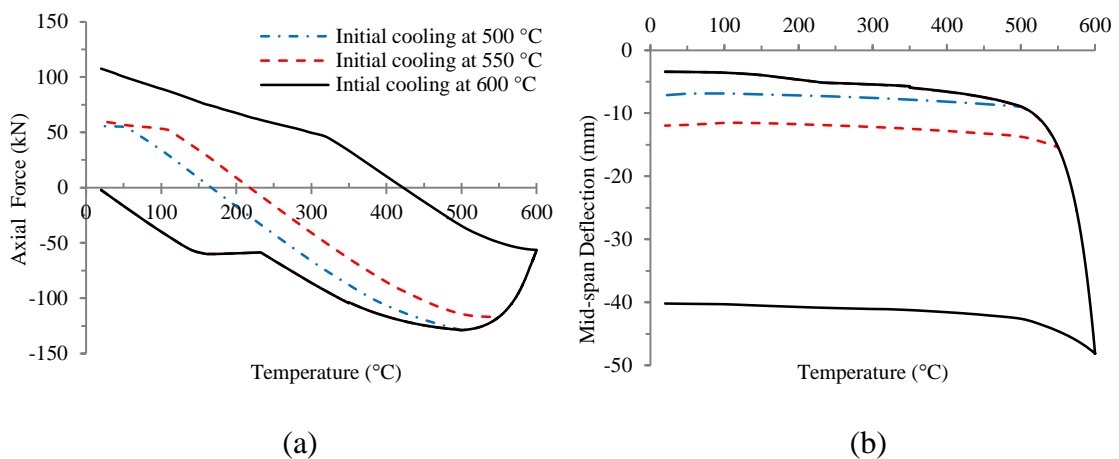


Figure. 22. Results for varying initial cooling temperatures following a heating rate of 20 °C/min: (a) beam axial force; (b) beam mid-span deflection.

e. Beam geometry

In this section, the beam geometry (e.g. size and length) is considered in order to have more insights on its effect on the creep response. A beam section of UB 305 × 102 × 25 is chosen to replace the existing beam under the same conditions and keeping the same setback distance. To maintain the same load ratio (half of the beam ambient plastic moment capacity) applied on the beam without increasing the shear force demand on the connection, the beam length is doubled from 2 to 4 meters in length while

maintaining the same applied force (40 kN). The FE results of different heating rates are presented in Fig. 23. A higher maximum beam axial force is reached in the heating phase since the beam length and section area are greater than that of the previous beam. Similarly, the beam mid-span deflection is also higher than that of the previous beam. Moreover, for the case of slow heating rate (5 °C/min), the axial force in the beam changes from compression to tension owing to the high beam deformation. Due to the fact that the setback distance is kept unchanged and the beam depth and length are increased, the beam comes in contact with the column at an earlier stage. Furthermore, lateral torsional buckling of the bottom flange and local buckling of the beam web near the shear tab are observed.

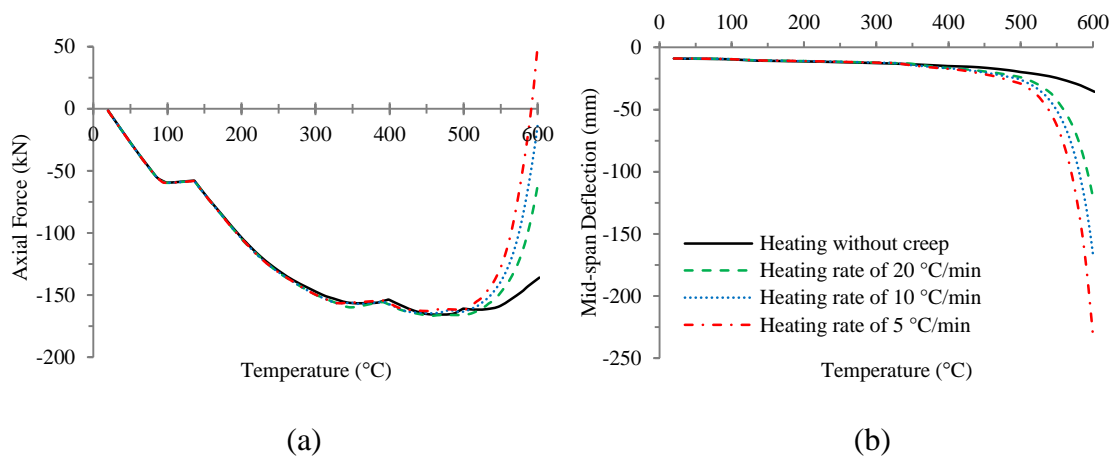


Figure. 23. Results of UB 305 × 102 × 25 beam for different heating rates: (a) beam axial force; (b) beam mid-span deflection.

f. Shear tab location

In the current design practice, the shear tab is typically shifted to the upper portion of the beam web. Three cases are considered to study the effect of the shear tab location on the performance of the frame in fire: 0, 25, and 50 mm above the beam center line. The beam in the previous section (UB 305 × 102 × 25) is used because it allows for

more space to move the shear tab away from the beam center line. The results are illustrated in Fig. 24. The results show that the location of the shear tab with respect to the beam center line does not have a significant effect on the results; however, slight changes can be observed. The more the distance between the shear tab plate and the beam center line increases, the earlier the beam bottom flange comes in contact with the column. This is evident since the contact angle decreases. Shifting the shear tab plate from the beam center line also results in an increase in the deflection at low temperatures. This can be related to the increase in the P- Δ effect explained previously. However, at late stages of fire, this behavior changes. It is observed that shifting the shear tab plate above the beam center line results in less mid-span deflection and less drop in the axial force. This can be attributed to the additional connection rotational stiffness (increase in the lever arm as the offset distance increases) following the beam-column contact.

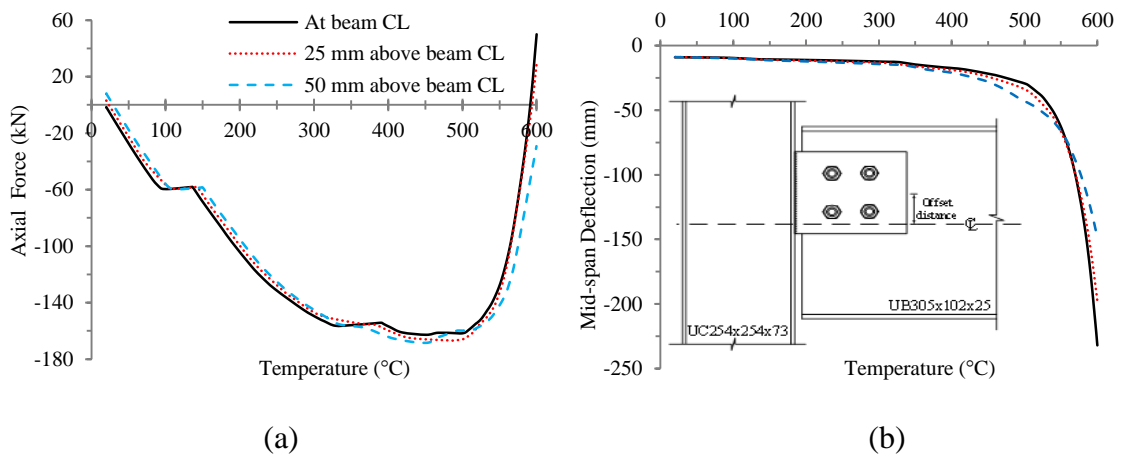


Figure. 24. Results of UB 305 × 102 × 25 beam with different shear tab locations: (a) beam axial force; (b) beam mid-span deflection.

CHAPTER VI

SUMMARY, CONCLUSIONS AND RECOMMENDATIONS

A. Summary and Conclusions

The behavior of steel structures in fire is of high complexity. Many factors and parameters contribute to the final response of the frame during fire events. The problem arises from the properties of the steel material which are greatly affected at high temperatures. The work presented in this thesis has been concerned with the development of a methodology to explicitly include the creep effect in ABAQUS FE models. The steps of including the time-dependent strains were thoroughly explained from which a subroutine was developed and incorporated in the FE simulations. The purpose of this study was to evaluate the influence of key parameters on the time-dependent behavior of steel frames with shear tab connections in fire using the developed subroutine. Extensive parametric studies were carried out after validating the FE models results against that of the experimental work available in literature. As it is clearly evident from the study, considering time and creep explicitly in structural fire analysis is of great importance especially when reaching high temperatures. Additionally, quantifying the effect of heating and cooling rates is not possible if creep is not introduced explicitly. The following points are to be concluded from this study:

- The developed user-defined subroutine can explicitly introduce creep strains in ABAQUS FE models under transient-state conditions of fire. The subroutine can account for the three factors affecting the creep strain rate development (temperature, stress, and time). It can be applied to any FE model in ABAQUS under certain conditions and limitations (material, temperature range...).

- Using a strain hardening formulation with implicit (backward Euler) integration method insures unconditionally stable results. However, small size increments are needed to get accurate results.
- Creep has a significant influence on the structure behavior at high temperatures. For restrained steel beams and under transient-state heating, it causes axial stress relaxation (decrease) and increases the mid-span deflection of the beam. Thus, ignoring the time-dependent strains at high temperatures can lead to under prediction of the beam deflection and over prediction of the axial thermal induced forces in restrained beams.
- According to the adopted creep model, by Fields and Fields (1989), the behavior of steel material is highly time-dependent for temperatures above 500 °C, where the great impact on steel elements behavior can be observed. Whereas, for temperatures below 400 °C, creep effect is not significant.
- The results show that as the heating rate decreases, the influence of creep effect increases, making it crucial to conduct time-dependent analyses when dealing with steel structures subjected to fire for long durations.
- Two column sizes were used in the study. The FE simulations showed that both columns resulted in relatively similar beam deflection. However, it was shown that the heavier column section can increase the induced axial force in the beam, thus increasing the development of creep strains.
- Slower heating rates, higher initial cooling temperatures, and longer cooling durations produce higher beam tensile force and larger mid-span deflection at the end of the cooling phase.

- In severe conditions, creep can alter the stability configuration of the structure. The load resisting mechanism can change from flexural to catenary action at high temperatures and stresses for a long period of time.
- In fire events, the shear tab connection region is subjected to high stresses making the development of creep strain significant at the connection region. This can be observed through the excessive bolt hole ovalization (elongation).
- When subjected to bending moment, creep strains cause axial stress redistribution over the beam cross section, relieving high axial stresses at the top and bottom fibers and redistributing them to the inner fibers to achieve equilibrium.
- The shear tab location, with respect to the beam center line has a slight effect on the beam behavior at early stages of fire. However, the results show that as the location of the shear tab moves above the beam center line, the deflection of the beam reduces due to the increased stiffness (lever arm) of the connection following the beam-column contact.

B. Recommendations

It is early at this stage to draw a generalized performance-based framework from the presented analyses. This study should be extended to develop a more simplified and practical models for fire structural design purposes. It is worth mentioning that most of the fire tests available in literature were conducted under fast heating regimes (i.e. using standardized temperature-time curves): exposing the tested specimens to short time periods during which creep strains can hardly develop. These standardized fire curves are not necessarily representative of time-temperature conditions that steel structures are exposed to in real fire scenarios. This implies that more experimental data and more

detailed computational studies are still needed to better understand the extent of which creep plays a role in affecting the steel behavior in fire. Further developments based on the presented analyses can be summarized in the following:

- A fracture model is needed to be adopted in all FE models which allows a post-yielding analysis of the connection response to fire.
- More work may be conducted to investigate the effect of thermal creep on the behavior of frames with different beam-column connections.
- Additional experimental work on full-scale tests with slow and medium heating rates is needed to be conducted for validation purposes.
- More reliable creep models should be developed to include the creep effect in other structural components (columns, bolts, welds...) as to study the global behavior of the system
- Creep effect should be studied at temperatures higher than 600 °C.

Ignoring the creep effect in structural fire analyses may lead to unsafe predictions of structural response when subjected to fire. In this regard, many efforts are being done to explicitly include creep in the performance-based structure-fire analyses to improve the representation of the true behavior of steel structures in fire.

BIBLIOGRAPHY

- ABAQUS ver. 6.14 documentation* (2014). Dassault Systemes Simulia Corporation.
- Dwaikat, M., & Kodur, V. (2010). "Effect of location of restraint on fire response of steel beams," *Fire Technology*, 46(1), 109-128.
- El Ghor, A. H., Hantouche, E. G., Morovat, M. A., & Engelhardt, M. (2016). Creep behavior of flush endplate connections at elevated temperatures due to fire. *Proceedings of the Structures in Fire Proceeding of the Ninth International Conference*.
- EN 1995-1-2 (2005). *Eurocode 3- design of steel structures - part 1-2: General rules - structural fire design*. European Committee for Standardization.
- Fields, A. B., & Fields, J. R. (1989). *Elevated temperature deformation of structural steel*. Gaithersburg, MD: NIST.
- Harmathy, T. Z. (1967). "A comprehensive creep model," *Journal of Basic Engineering*, 89(3), 496–502.
- Hu, G., & Engelhardt, D. M. (2014). "Experimental investigation of steel single plate beam end connections at elevated temperatures," *Engineering Structures*, 58, 141-151.
- Hu, Y., Davison, B. J., Burgess, W. I., & Plank, R. J. (2007). Comparative study of the behaviour of BS 4190 and BS EN ISO 4014 bolts in fire. *Proceedings of the 3rd International Conference on Steel and Composite Structures*, London, 587–592.
- Huang, Z., & Tan, K. (2004). "Effects of external bending moments and heating schemes on the responses of thermally restrained steel columns," *Engineering Structures*, 26(6), 769-780.
- Huang, Z., Tan, K., & Ting, S. (2006). "Heating rate and boundary restraint effects on fire resistance of steel columns with creep," *Engineering Structures*, 28(6), 805-817.
- Jabotian, H. V., & Hantouche, E. G. (2018). "Thermal creep effect on the behavior of shear tab connections due to fire temperatures," *Fire Safety Journal*, 96, 74-92.
- Kodur, V., & Dwaikat, M. (2010). "Effect of high temperature creep on the fire response of restrained steel beams," *Materials and Structures*, 43(10), 1327-1341.
- Kodur, V., Dwaikat, M., & Fike, R. (2010). "High-temperature properties of steel for fire resistance modeling of structures," *Journal of Materials in Civil Engineering*, 22(5), 423-434.

- Lee, J., Morovat, M. A., Hu, G., Engelhardt, M. D., & Taleff, E. M. (2013). "Experimental investigation of mechanical properties of ASTM A992 steel at elevated temperatures," *Engineering Journal*, 50(4), 249-272.
- Li, G., & Zhang, C. (2012). "Creep effect on buckling of axially restrained steel columns in real fires," *Journal of Constructional Steel Research*, 71, 182-188.
- Lie, T. T. (1992). *Structural fire protection*. New York: American Society of Civil Engineers.
- Luecke, W. E., McColskey, J. D., McCowan, C. N., Banovic, S. W., Fields, R. J., Foecke, T. J., Siewert, T. A., & Gayle, F. W. (2005). *Federal building and fire safety investigation of the world trade center disaster - mechanical properties of structural steels*. Report NIST NCSTAR 1-3D, National Institute of Standards and Technology.
- Matar, M., Rahman, A., & Shrih, A. (2014). "Primary creep in ASTM A325 bolts under simulated fire loading," *International Journal of Engineering Research & Innovation*, 6(1), 28-33.
- Morovat, M. A. (2014). *Creep buckling behavior of steel columns subjected to fire*.
- Morovat, M. A., El Ghor, A. H., & Hantouche, E. G. (2018). "Time-dependent response of flush endplate connections to fire temperatures," *Journal of Structural Engineering*, 144(4), 04018023.
- Morovat, M. A., Engelhardt, D. M., Helwig, T., & Taleff, E. (2014). "High-temperature creep buckling phenomenon of steel columns subjected to fire," *Journal of Structural Fire Engineering*, 5(3), 189-202.
- Morovat, M. A., Engelhardt, M. D., Taleff, E. M., & Helwig, T. (2011). "Importance of time-dependent material behavior in predicting strength of steel columns exposed to fire," *Applied Mechanics and Materials*, 82, 350.
- Naumenko, K., & Altenbach, H. (2007). *Modeling of creep for structural analysis*. Berlin, Heidelberg: Springer-Verlag.
- Newman, M. G., Robinson, T. J., & Bailey, G. C. (2000). *Fire safe design: A new approach to multi-storey steel-framed buildings*.
- Pakala, P., & Kodur, V. (2016). "Effect of concrete slab on the behavior of fire exposed subframe assemblies with bolted double angle connections," *Engineering Structures*, 107, 101-115.
- Poh, K. W. (2001). "Stress-strain-temperature relationship for structural steel," *Journal of Materials in Civil Engineering*, 13(5), 371-379.
- Selamet, S., & Garlock, M. (2010). "Robust fire design of single plate shear connections," *Engineering Structures*, 32, 2367-2378.

- Sleiman, S. A., & Hantouche, E. G. (2015). Isolated shear endplate and double angle connections: Prediction of strength capacity. *Proceedings of the Structures Congress 2015*, 2153-2163.
- Sunder, S. S. (2005). *Final report on the collapse of the world trade center towers :: Federal building and fire safety investigation of the world trade center disaster*. National Institute of Standards and Technology.
- Tan, H. K., Ting, K. S., & Huang, F. Z. (2002). "Visco-elasto-plastic analysis of steel frames in fire," *Journal of Structural Engineering*, 128(1), 105-114.
- Torić, N., Harapin, A., & Boko, I. (2013a). "Experimental verification of a newly developed implicit creep model for steel structures exposed to fire," *Engineering Structures*, 57, 116-124.
- Torić, N., Harapin, A., & Boko, I. (2013b). "Modelling of steel creep at high temperatures using an implicit creep model," *Key Engineering Materials*, 553, 13-22.
- Wald, F., Simões da Silva, L., Moore, D. B., Lennon, T., Chladná, M., Santiago, A., Beneš, M., & Borges, L. (2006). "Experimental behaviour of a steel structure under natural fire," *Fire Safety Journal*, 41(7), 509-522.
- Wang, W., Yan, S., & Kodur, V. (2016). "Temperature induced creep in low-alloy structural Q345 steel," *Journal of Materials in Civil Engineering*, 28(6), 06016003.
- Wang, Y. C., Dai, X. H., & Bailey, C. G. (2011). "An experimental study of relative structural fire behaviour and robustness of different types of steel joint in restrained steel frames," *Journal of Constructional Steel Research*, 67(7), 1149-1163.
- Williams-leir, G. (1983). "Creep of structural steel in fire: Analytical expressions," *Fire and Materials*, 7(2), 73-78.
- Yang, K., & Yu, Z. (2013). "Experimental research on the creep buckling of fire-resistant steel columns at elevated temperature," *Steel and Composite Structures*, 15(2), 163-173.
- Yu, H., Burgess, I. W., Davison, J. B., & Plank, R. J. (2009a). "Experimental investigation of the behaviour of fin plate connections in fire," *Journal of Constructional Steel Research*, 65(3), 723-736.
- Yu, H., Burgess, I. W., Davison, J. B., & Plank, R. J. (2009b). "Tying capacity of web cleat connections in fire, part 1: Test and finite element simulation," *Engineering Structures*, 31(3), 651-663.

APPENDIX

ABAQUS USER-DEFINED SUBROUTINES (CREEP)

A. Steady-state analysis (for 550 °C)

```
SUBROUTINE CREEP (DECRA, DESWA, STATEV, SERD, EC, ESW, P, QTILD,  
1 TEMP, DTEMP, PREDEF, DPRED, TIME, DTIME, CMNAME, LEXIMP, LEND,  
2 COORDS, NSTATV, NOEL, NPT, LAYER, KSPT, KSTEP, KINC)  
  
C  
C INCLUDE 'ABA_PARAM.INC'  
C  
C CHARACTER*80 CMNAME  
C  
C DIMENSION DECRA (5), DESWA (5), STATEV (*), PREDEF (*), DPRED (*),  
1 TIME (3), COORDS (*), EC (2), ESW (2)  
C  
C DEFINE CONSTANTS  
C  
C A = 31.22319223  
C XN = 5.62  
C XM = -0.175  
C C1=1./ (1.+XM)  
C  
C IF (LEXIMP.EQ.0) THEN  
C EC0=EC (1)  
C TERM1=(A*QTILD**XN*C1)**C1  
C TERM2=TERM1*DTIME+EC0**C1  
C DECRA (1) = (TERM2** (1.+XM) -EC0)  
C  
C END IF  
C  
C IF (LEXIMP.EQ.1) THEN  
C EC0=EC (1)  
C TERM1=(A*QTILD**XN*C1)**C1  
C TERM2=TERM1*DTIME+EC0**C1  
C DECRA (1) = (TERM2** (1.+XM) -EC0)  
C DECRA (5) =XN*DTIME*TERM2**XM*TERM1/QTILD  
C END IF  
C  
C RETURN  
C END
```


B. Stepwise steady-state analysis

```
SUBROUTINE CREEP (DECRA, DESWA, STATEV, SERD, EC, ESW, P, QTILD,  
1 TEMP, DTEMP, PREDEF, DPRED, TIME, DTIME, CMNAME, LEXIMP, LEND,  
2 COORDS, NSTATV, NOEL, NPT, LAYER, KSPT, KSTEP, KINC)  
  
C  
  INCLUDE 'ABA_PARAM.INC'  
  
C  
  CHARACTER*80 CMNAME  
  
C  
  DIMENSION DECRA (5), DESWA (5), STATEV (*), PREDEF (*), DPRED (*),  
1 TIME (3), COORDS (*), EC (2), ESW (2)  
C DEFINE CONSTANTS  
  IF (TEMP<450) THEN  
    A = 0.143754956  
    XN = 4.66  
    XM = -0.7  
    C1=1./ (1.+XM)  
  END IF  
  IF (TEMP>=450.AND.TEMP<500) THEN  
    A = 0.578587582  
    XN = 4.98  
    XM = -0.525  
    C1=1./ (1.+XM)  
  END IF  
  IF (TEMP>=500.AND.TEMP<550) THEN  
    A = 1.878290592  
    XN = 5.3  
    XM = -0.35  
    C1=1./ (1.+XM)  
  END IF  
  IF (TEMP>=550.AND.TEMP<600) THEN  
    A = 31.22319223  
    XN = 5.62  
    XM = -0.175  
    C1=1./ (1.+XM)  
  END IF  
  IF (TEMP>=600.AND.TEMP<650) THEN  
    A = 495.6753044  
    XN = 5.94  
    XM = 0  
    C1=1./ (1.+XM)  
  END IF  
  IF(LEXIMP.EQ.0) THEN  
    EC0=EC (1)  
    TERM1=(A*QTILD**XN*C1)**C1  
    TERM2=TERM1*DTIME+EC0**C1  
    DECRA (1) = (TERM2** (1.+XM) -EC0)  
  END IF  
  IF(LEXIMP.EQ.1) THEN  
    EC0=EC (1)  
    TERM1=(A*QTILD**XN*C1)**C1  
    TERM2=TERM1*DTIME+EC0**C1  
    DECRA (1) = (TERM2** (1.+XM) -EC0)  
    DECRA (5) =XN*DTIME*TERM2**XM*TERM1/QTILD  
  END IF  
  RETURN  
END
```

C. Transient-state analysis

```
SUBROUTINE CREEP (DECRA, DESWA, STATEV, SERD, EC, ESW, P, QTILD,  
1 TEMP, DTEMP, PREDEF, DPRED, TIME, DTIME, CMNAME, LEXIMP, LEND,  
2 COORDS, NSTATV, NOEL, NPT, LAYER, KSPT, KSTEP, KINC)  
  
C  
  INCLUDE 'ABA_PARAM.INC'  
  
C  
  CHARACTER*80 CMNAME  
  
C  
  DIMENSION DECRA(5), DESWA(5), STATEV(*), PREDEF(*), DPRED(*),  
1 TIME(3), COORDS(*), EC(2), ESW(2)  
  
C  
C DEFINE CONSTANTS  
  
  XN = 2.1+0.0064*TEMP  
  XM = -1.1+0.0035*TEMP-1  
  IF (TEMP<=350) THEN  
    A = 0  
  END IF  
  IF (TEMP>350.AND.TEMP<500) THEN  
    A = (10**(-6.1-0.00573*TEMP)/100) * (145.03774**XN) * (XM+1)  
  END IF  
  IF (TEMP>=500) THEN  
    A = (10**(-13.25+0.00851*TEMP)/100) * (145.03774**XN) * (XM+1)  
  END IF  
  C1=1./(1.+XM)  
  
C Incremental creep strain difference  
  
  IF(LEXIMP.EQ.0) THEN  
    EC0=EC(1)  
    TERM1=(A*QTILD**XN*C1)**C1  
    TERM2=TERM1*DTIME+EC0**C1  
    DECRA(1)=(TERM2**(1.+XM)-EC0)  
  
  END IF  
  
C  
  IF(LEXIMP.EQ.1) THEN  
    EC0=EC(1)  
    TERM1=(A*QTILD**XN*C1)**C1  
    TERM2=TERM1*DTIME+EC0**C1  
    DECRA(1)=(TERM2**(1.+XM)-EC0)  
    DECRA(5)=XN*DTIME*TERM2**XM*TERM1/QTILD  
  END IF  
  
C  
  RETURN  
  END
```

LIST OF THE FE SIMULATIONS

Table 2. Summary of the FE simulations developed in ABAQUS

	Tests	Column section	Beam section	Heating Phase			Cooling Phase		
				Target temperature (°C)	Time / rate	Creep effect	Target temperature (°C)	Time (min.)	Creep effect
Validation	1	UC 254x254x73	UB 178x102x19	800	-	✘	20	-	✘
	2	UC 152x152x23	UB 178x102x19	800	-	✘	20	-	✘
Steady-state analysis	3	UC 254x254x73	UB 178x102x19	400	120 min	✓	-	-	-
	4	UC 254x254x73	UB 178x102x19	450	120 min	✓	-	-	-
	5	UC 254x254x73	UB 178x102x19	500	120 min	✓	-	-	-
	6	UC 254x254x73	UB 178x102x19	550	120 min	✓	-	-	-
	7	UC 254x254x73	UB 178x102x19	600	120 min	✓	-	-	-
Stepwise steady-state analysis	8	UC 254x254x73	UB 178x102x19	600	5 min/step	✓	-	-	-
	9	UC 254x254x73	UB 178x102x19	600	10 min/step	✓	-	-	-
Transient-state analysis	10→13	UC 254x254x73	UB 178x102x19	600	-	✘	20	0,5,10 and 20	✓
	14→17	UC 254x254x73	UB 178x102x19	600	5 °C/min	✓	20	0,5,10 and 20	✓
	18→21	UC 254x254x73	UB 178x102x19	600	10 °C/min	✓	20	0,5,10 and 20	✓
	22→25	UC 254x254x73	UB 178x102x19	600	20 °C/min	✓	20	0,5,10 and 20	✓
	26→29	UC 254x254x73	UB 178x102x19	550	-	✘	20	0,5,10 and 20	✓
	30→33	UC 254x254x73	UB 178x102x19	550	5 °C/min	✓	20	0,5,10 and 20 min	✓
	34→37	UC 254x254x73	UB 178x102x19	550	10 °C/min	✓	20	0,5,10 and 20	✓
	38→41	UC 254x254x73	UB 178x102x19	550	20 °C/min	✓	20	0,5,10 and 20	✓
	42→45	UC 254x254x73	UB 178x102x19	500	-	✘	20	0,5,10, and 20 min	✓
	46→49	UC 254x254x73	UB 178x102x19	500	5 °C/min	✓	20	0,5,10 and 20	✓
	50→53	UC 254x254x73	UB 178x102x19	500	10 °C/min	✓	20	0,5,10 and 20	✓
	54→57	UC 254x254x73	UB 178x102x19	500	20 °C/min	✓	20	0,5,10 and 20	✓
	58→61	UC 152x152x23	UB 178x102x19	600	-	✘	20	0,5,10 and 20	✓

62→65	UC 152x152x23	UB 178x102x19	600	5 °C/min	✓	20	0,5,10 and 20	✓
66→69	UC 152x152x23	UB 178x102x19	600	10 °C/min	✓	20	0,5,10 and 20	✓
70→73	UC 152x152x23	UB 178x102x19	600	20 °C/min	✓	20	0,5,10 and 20	✓
74→77	UC 254x254x73	UB 305x102x25	600	-	✘	20	0,5,10 and 20	✓
78→81	UC 254x254x73	UB 305x102x25	600	5 °C/min	✓	20	0,5,10 and 20	✓
82→85	UC 254x254x73	UB 305x102x25	600	10 °C/min	✓	20	0,5,10 and 20 min	✓
86→89	UC 254x254x73	UB 305x102x25	600	20 °C/min	✓	20	0,5,10 and 20 min	✓
90→92	UC 254x254x73	UB 305x102x25 (3 shear tab locations)	600	20 °C/min	✓	-	-	✘

